From THE DEPARTMENT OF CLINICAL NEUROSCIENCE
Karolinska Institutet, Stockholm, Sweden

IN VIVO AND IN VITRO STUDIES OF THE SEROTONIN 1B RECEPTOR IN RELATION TO MAJOR DEPRESSIVE DISORDER AND TREATMENT WITH KETAMINE

Emma R. Veldman

Karolinska Institutet

Stockholm 2021

Published by Karolinska Institutet.
Printed by Universitetsservice US-AB, 2021

ISBN 978-91-8016-077-3
Cover illustration: 3D-rendered PET image of the radioligand [^{11}C]AZ10419369 binding to the serotonin 1B receptor. The images show an average of data from 52 healthy subjects from a sagittal and axial view. Created using 3D Slicer (www.slicer.org)

In Vivo and In Vitro Studies of the Serotonin 1B Receptor in Relation to Major Depressive Disorder and Treatment with Ketamine
THESIS FOR DOCTORAL DEGREE (Ph.D.)

By

Emma R. Veldman

The thesis will be defended in public in Inghesalen, Widerströmska Huset, Tomtebodavägen 18a, Solna, on February 12, at 14:00.

Principal Supervisor:
Dr. Johan Lundberg
Karolinska Institutet
Department of Clinical Neuroscience

Co-supervisor(s):
Dr. Andrea Varrone
Karolinska Institutet
Department of Clinical Neuroscience

Dr. Marie Svedberg
Sophia Hemmet Högskola
Department of Health Promotion

Prof. Per Svenningsson
Karolinska Institutet
Department of Clinical Neuroscience

Opponent:
Dr. Rupert Lanzenberger
Medical University Vienna
Department of Psychiatry and Psychotherapy

Examination Board:
Prof. Mathias Hallberg
Uppsala Universitet
Department of Pharmaceutical Biosciences

Prof. Julie Price
Harvard Medical School
Department of Radiology

Prof. Fredrik Piehl
Karolinska Institutet
Department of Clinical Neuroscience

ABSTRACT

Despite the large implications of Major Depressive Disorder (MDD) on disease burden worldwide, current treatment options are suboptimal and a third of patients suffering from this disease do not respond to treatment. Therefore, an unmet need exists for the development of new treatment options and methods to aid appropriate treatment selection in individual patients. Selection of suitable biomarkers and reliable quantification methods are essential steps in this process. In recent research on MDD, more interest has arisen for the serotonin 1B (5-HT_{1B}) receptor and for ketamine as a new antidepressant treatment option. This thesis focuses on the involvement of the 5-HT_{1B} receptor and the related protein p11 in the pathophysiology of MDD and the antidepressant mechanism of action of ketamine. For quantification of 5-HT_{1B} receptor densities, the nuclear imaging techniques Autoradiography (ARG) and Positron Emission Tomography (PET) were used. This work includes the development and application of an improved method for quantification of 5-HT_{1B} receptor binding using PET. Quantification of p11 levels was performed in specific cell populations using Flow Cytometry.

In study I, 5-HT_{1B} receptor binding densities and cortical distribution were examined using ARG in anterior cingulate cortex tissue of subjects with MDD, schizophrenia, bipolar disorder and healthy controls. Binding of the radioligand [^{3}H]AZ10419369 in tissue of in total 52 subjects showed no significant differences between the subject groups. A distribution pattern with higher 5-HT_{1B} receptor binding in supragranular layer compared to the infragranular layer was found, which correlated with glutamatergic N-methyl-D-aspartate receptor distribution. Female subjects had lower 5-HT_{1B} receptor densities than male subjects, which was mostly profound in the MDD group.

In study II, an improved method was developed for delineation of Volumes of Interest (VOIs) for PET data with the radioligand [^{11}C]AZ10419369. Based on a 3D [^{3}H]AZ10419369 ARG model in *post mortem* brainstem tissue and literature findings, appropriate VOIs for quantification in PET were selected. Two previously developed semi-automatic VOI delineation methods, based on template or individual data, were evaluated on test-retest data of 8 healthy subjects and showed improved reliability compared to a conventional manual VOI. The VOIs created with PET template data of 52 healthy subjects can be automatically applied to future PET studies measuring 5-HT_{1B} receptor binding in the brainstem.

Furthermore, in a randomized placebo-controlled study the effect of ketamine on cerebral [^{11}C]AZ10419369 PET binding (study III) and peripheral p11 protein levels measured with Flow Cytometry (study IV) were examined in patients with Selective Serotonin Reuptake Inhibitor (SSRI) resistant MDD. An increase in 5-HT_{1B} binding in the hippocampus and a decrease in p11 levels in both cytotoxic T cells and T-helper cells populations were seen in the ketamine group (n=20), although both did not differ from changes seen in the placebo group (n=10). Changes in Montgomery-Åsberg Depression Rating Scale (MADRS) score after ketamine treatment correlated significantly with baseline 5-HT_{1B} receptor binding in the ventral striatum and baseline p11 levels in cytotoxic T cells. Future studies should be conducted on the role of 5-HT_{1B} receptors and p11 in the antidepressant mechanism of action of ketamine and should clarify if these proteins could be used as biomarkers to predict ketamine treatment response in subjects with SSRI-resistant MDD.

LIST OF SCIENTIFIC PAPERS

I. **Veldman ER***, Svedberg MM*, Svenningsson P, Lundberg J (2017) Distribution and levels of 5-HT1B receptors in anterior cingulate cortex of patients with bipolar disorder, major depressive disorder and schizophrenia – An autoradiography study. *European Neuropsychopharmacology*, 27(5):504-514

II. **Veldman ER**, Varrone A, Varnäs K, Svedberg MM, Cselényi Z, Tiger M, Gulyas B, Halldin C, Lundberg J. Serotonin 1B receptor density mapping of the human brainstem using Positron Emission Tomography and Autoradiography. *Manuscript*

III. Tiger M, **Veldman ER**, Ekman CJ, Halldin C, Svenningsson P, Lundberg J (2020). A randomized placebo-controlled PET study of ketamine´s effect on serotonin1B receptor binding in patients with SSRI-resistant depression. *Translational Psychiatry* 10(159)

IV. **Veldman ER***, Mamula D*, Jiang H*, Tiger M, Ekman CJ, Lundberg J, Svenningsson P. P11 (S100A10) as a potential predictor of ketamine response in patients with SSRI-resistant depression. *Under review*

* *These authors contributed equally to this work*

SCIENTIFIC PAPERS NOT INCLUDED IN THE THESIS

Veldman ER, Jia Z, Halldin C, Svedberg MM (2016). Amyloid binding properties of curcumin analogues in Alzheimer's disease postmortem brain tissue. *Neuroscience Letters* 630:183–188

Tangen Ä, **Veldman ER**, Svensson J, Tiger M, Nord M, Sorjonen K, Andersson M, Plavén-Sigray P, Varrone A, Halldin C, Varnäs K, Borg J, Lundberg J. Associations between cognition and serotonin 1B binding in control subjects – A [^{11}C]AZ10419369 Positron Emission Tomography study. *Manuscript*

Tangen Ä, **Veldman ER**, Svensson J, Tiger M, Nord M, Andersson M, Sorjonen K, Plavén-Sigray P, Varrone A, Halldin C, Varnäs K, Borg J, Lundberg J. Associations between autism-related cognitive functioning and regional binding of 5-HTT and 5-HT_{1B} receptor in neurotypical control subjects. *Manuscript*

CONTENTS

LIST OF ABBREVIATIONS

^{11}C	Carbon-11
^{18}F	Fluor-18
^{3}H	Tritium (Hydrogen-3)
5-HT	Serotonin
5-HTT	Serotonin transporter
ACC	Anterior Cingulate Cortex
AMPA	α-amino-3-hydroxy-5-methylisoxazole-4-propionic acid
APD	Absolute Percentage Difference
ARG	Autoradiography
BBB	Blood-Brain Barrier
B_{max}	Baximum density of binding sites
B_{avail}	Density of available binding sites
BP_{ND}	Non-Displaceable Binding Potential
$CD4^+$ cell	T-helper cell
$CD8^+$ cell	Cytotoxic T cell
C_x	Radioligand concentration in compartment “X”
CNS	Central Nervous System
COV	Coefficient of Variation
f_{ND}	Fraction of free radioligand in the non-displaceable compartment
FSC	Forward Scatter
HRRT	High-Resolution Research Tomograph
ICC	Intraclass Correlation Coefficient
K_d	Equilibrium dissociation rate constant
k_x	Rate constant “x" (min^{-1})
MADRS	Montgomery Åsberg Depression Rating Scale
MD	Minimal Detectable difference
MDD	Major Depressive Disorder
MFI	Median Fluorescence Intensity
MNI	Montréal Neurological Institute

MRI	Magnetic Resonance Imaging
NK cell	Natural Killer cell
NMDA	N-methyl-D-aspartate
PBMC	Peripheral Blood Mononuclear Cell
PET	Positron Emission Tomography
PMI	Post Mortem Interval
PVE	Partial Volume Effect
ROI	Region of Interest
SSC	Side scatter
SEM	Standard Error of Measurement
SI	Separation Index
SSRI	Selective Serotonin Reuptake Inhibitor
SRTM	Simplified Reference Tissue Model
SUV	Standard Uptake Value
TAC	Time Activity Curve
VOI	Volume of Interest
VST	Ventral Striatum
WAPI	Wavelet-Aided Parametric Imaging

INTRODUCTION

1.1 RATIONALE FOR THE THESIS

Major depressive disorder (MDD) is the most common psychiatric disorder and a leading cause of disability worldwide that affects around 4.4% of the global population[1]. Despite the availability of various antidepressant treatment options, treatment success in MDD is limited[2]. About 30% of MDD patients need to try out multiple treatments before getting into remission and even more than 30% of MDD patients do not achieve remission at all, i.e. these patients are considered to have treatment-resistant depression[3,4]. Most MDD patients who do get into remission experience a relapse within 1-2 years[4]. Therefore, there is a large unmet need for improved treatment options, as well as improved methods to select effective treatments for individual patients. Relatively few new antidepressant drugs have been discovered in recent years[5], which is likely caused by the insufficient understanding of the pathophysiology of MDD. The identification of reliable biomarkers is an important step in the process of improving knowledge on pathophysiology and the mechanism of antidepressants.

Currently, the pharmacological treatment of MDD is primarily based on targeting the monoaminergic system. A common target for antidepressants is the serotonin transporter (5-HTT), e.g. Selective Serotonin Reuptake Inhibitors (SSRIs). Because of a large proportion of treatment-resistant MDD subjects, drug development should probably be focused on a different target. The serotonin 1B (5-HT_{1B}) receptor and its interaction with the protein p11 have recently received more interest as a possible target for pharmacological treatment of psychiatric disorders and seem interesting candidates as biomarkers for MDD.

An important breakthrough in antidepressant drug development has been the coincidental finding of the antidepressant side effect of the analgesic drug ketamine[6,7]. However, its clinical implementation is limited by numerous other short-term and long-term side effects[8]. For the development of more suitable treatment options, it is highly desired to unravel the antidepressant mechanism of action of ketamine. Moreover, clinical decision making for this treatment option could be optimized when a biomarker for prediction of treatment outcomes becomes available.

Neuropsychiatric research is challenging due to the complexity and low accessibility of the brain. Nuclear imaging techniques, such as Autoradiography (ARG) and Positron Emission Tomography (PET), are useful to retrieve biological insights of the brain *in vitro* and *in vivo*, respectively. Both ARG and PET enable accurate determination of protein levels in the brain. Relatively low resolution and high costs are limitations of PET, but this can partly be overcome by improved quantification methods which increase the reliability of outcomes and reduce the number of study subjects needed in future studies. ARG complements PET with its high resolution and possibility to examine receptor distribution in a controlled lab environment. While PET and ARG are excellent technique to study processes directly in the brain, a biomarker accessible in peripheral blood would be preferred for both patient comfort and implementation in clinical practice. Flow Cytometry can be used to quantify potential biomarkers in specific cell types, e.g. peripheral blood mononuclear cells.

The general aim of this thesis was to study the 5-HT_{1B} receptor and p11 protein in MDD and treatment with ketamine. This was achieved by using *in vivo* PET and *in vitro* ARG and Flow Cytometry. Moreover, ARG was used to complement PET in the development of an improved quantification method.

1.2 MAJOR DEPRESSIVE DISORDER

MDD is characterized by depressed mood, anhedonia, fatigue, impaired attention control and disturbances in weight, sleep and movement[9]. The exact mechanisms underlying the disease process and current treatment options are still to a large extent unclear. Several systems and processes are suggested to be involved in the pathophysiology of MDD, among others: the hypothalamic-pituitary-adrenal axis, which regulates stress response; the immune system; neuroplasticity, i.e. the ability to grow and reorganize neuronal cells; and the monoaminergic neurotransmitter system in the central nervous system (CNS)[10,11]. Currently, guidelines in clinical practice suggest treatment for MDD with psychotherapy or pharmaceutical treatment interacting with the monoaminergic system, especially noradrenalin, serotonin (5-hydroxytryptamine, 5-HT) and dopamine[12].

An association between MDD and the monoaminergic system was suggested after the discovery of the relation between the antidepressant side effect of the anti-hypertensive drug reserpine and monoamine depletion[13]. The role of serotonin in MDD was further supported by antidepressive agents that increased available serotonin concentrations[14,15] and the effect of tryptophan (a serotonin precursor) depletion on relapse in MDD patients[16]. Studies in which levels of serotonin metabolites in plasma and *post mortem* tissue of patients with MDD were measured, did not provide definitive findings in relation to MDD[10]. Serotonergic neurotransmitter function in MDD is therefore thought to be impaired by malfunctioning of receptors and downstream mechanisms[11].

1.3 THE SEROTONIN SYSTEM

1.3.1 Overview of the serotonin system

Serotonin is a neurotransmitter involved in the vast majority of behavioral processes, although most serotonin receptors are found outside the CNS, e.g. in blood vessels and the gastrointestinal tract[17]. In the CNS, serotonin neurons originate in brainstem nuclei (Figure 1), where they are mostly situated in three separate regions close to the midline, i.e. the *raphe nuclei*: the caudally located raphe nuclei and the two rostrally located median and dorsal raphe nuclei. The two largest caudally located raphe nuclei are the raphe magnus and the raphe obscurus, which project towards the spinal cord. The median and dorsal nuclei both project to most subcortical and cortical regions; the striatum and hippocampus are nearly exclusively innervated by the dorsal and median raphe nuclei, respectively[18].

Serotonin receptors can be divided into 7 subgroups, based on their pharmacological profile, which can be subcategorized resulting in 14 currently known types of serotonin receptors[19]. These receptors are G-protein coupled receptors, except for the ligand-gated ion channel 5-HT_3

receptor[19]. Previous studies in MDD subjects showed alterations in 5-HTT[20], 5-HT_{1A} receptor[21] and 5-HT_{2A} receptor[22] concentrations compared to control subjects. The 5-HT_{1B} receptor currently receives increasing interest in research of the pathophysiology and treatment of MDD[23,24].

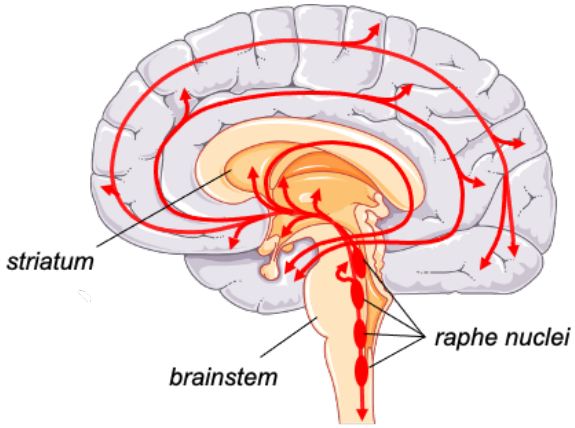

Figure 1: Serotonergic nuclei in the brainstem (*raphe nuclei*) and projections (red arrows) towards cortical (purple area) and subcortical regions. Figure created by using an image from Servier Medical Art (http://smart.servier.com/), licensed under CC BY 3.0

1.3.2 Serotonin 1B receptor

5-HT_{1B} receptors are $G_{i/o}$-protein coupled and occur as both auto- and heteroreceptors, thereby inhibiting the release of respectively serotonin and other neurotransmitters[25]. In the central nervous system, the receptor is most abundant in the globus pallidus and substantia nigra[26–28], whereas 5-HT_{1B} mRNA is absent in these regions and instead found in high concentrations in the striatum and cortex[26,27]. This minimal co-localization is likely caused by the receptors' predominant localization on axon terminals[26].

In animals, low 5-HT_{1B} receptor activation has been linked to aggression[29] and anxiety[30]. Moreover, human PET studies showed an association with anger[31] and creative ability[32].

The link between the 5-HT_{1B} receptor and MDD is well-studied, although findings are not always consistent. 5-HT_{1B} receptor knock-out mice were shown to have less depressive symptoms compared to controls[33]. Moreover, increased 5-HT_{1B} receptor levels were found throughout the brain in an animal model of MDD compared to controls[34,35]. However, reduced levels of 5-HT_{1B} receptors in the hippocampus were associated with genetic and environmental vulnerability for MDD in rats[36]. Studies on 5-HT_{1B} receptor mRNA expression in the raphe nuclei of rodents also seem conflicting, with increases in 5-HT_{1B} receptor mRNA expression both being associated with MDD[37] and with a protective function in MDD[38,39]. The discrepancy in these findings could be, among others, explained by the differences in MDD models used, analysis methods or heterogeneity within the studied regions.

In humans, a polymorphism of the 5-HT_{1B} receptor G861C gene has been associated with MDD[40]. In *post mortem* cortical tissue[41], decreased 5-HT_{1B} mRNA levels were found in suicide victims compared to tissue originating from healthy controls. In the anterior cingulate cortex of MDD subjects, mRNA levels were found to be lower compared to subjects with schizophrenia and bipolar disorder[42]. *In vivo* studies in MDD subjects showed lower 5-HT_{1B}

receptor availability in hippocampus, anterior cingulate cortex[43] and a volume containing the ventral striatum and pallidum[44] compared to healthy control subjects.

The 5-HT_{1B} receptor has also been implicated in treatment of MDD. A reduction of 5-HT_{1B} receptor availability was seen after treatment of MDD patients with cognitive behavior therapy[45]. Treatment with both 5-HT_{1B} receptor agonists and antagonists has been associated with antidepressive effects[46], possibly due to a difference in targeting either 5-HT_{1B} auto- or hetero-receptors[24]. A commonly used antidepressant which acts as partial agonist towards the 5-HT_{1B} receptor[47] is vortioxetine. Vortioxetine has been shown to bind to the 5-HT_{1B} receptor in the non-human primate brain *in vivo* at clinically relevant doses[48], although it is unclear to what extent this contributes to the antidepressant effect in humans.

1.3.3 P11

The protein P11 (S100-A10) plays a crucial role in 5-HT_{1B} receptor functioning: the protein increases localization of the 5-HT_{1B} receptor on the cell membrane and enhances its function[49]. P11 is a member of the calcium binding s-100 protein family[50] and is also found to interact with 5-HT_{1D}[49], 5-HT_4[51], metabotropic glutamate 5[52], CC chemokine 10 receptors[53] and various ion channels[54,55]. P11 is mostly found in the lungs, intestines and kidneys[56]. In the brain, p11 has a widespread distribution, although in lower concentrations[56,57]. Next to this, its presence is confirmed in peripheral blood mononuclear cells (PBMCs)[58,59], with a 10-fold higher magnitude presence in monocytes[59].

Knockout of the p11 gene in mice was shown to exhibit a depressive-like phenotype, whereas the overexpression of p11 levels induced behavioral effects which are also seen after antidepressant treatment[49]. Moreover, administration of the antidepressant compounds imipramine or tranylcypromine, in combination with electroconvulsive shocks, increased p11 mRNA in the cortex of mouse models of depression[49]. More recent studies have found that the induction of a depression-like behavior by p11 reduction is dependent on localization and cell type[52,55,60].

P11 mRNA expression in human MDD subjects was found to be decreased in frontocortical areas, the hippocampus, amygdala[41] and anterior cingulate cortex (ACC)[49]. Likewise, reductions in p11 protein levels were found in the ACC[49] and nucleus accumbens[60] of MDD subjects compared to healthy control subjects.

Interestingly, compared to findings in cerebral tissue, an opposite pattern seems to occur in peripheral blood: p11 mRNA expression and p11 protein levels in PBMCs were shown to be increased in MDD subjects compared to healthy subjects[58]. Likewise, protein p11 levels in PBMCs of Parkinson subjects with depression were increased in classically activated monocytes and cytotoxic T cells compared to healthy subjects[61]. Treatment with the SSRI citalopram showed an early reduction of p11 levels in monocytes and Natural Killer (NK) cells, which was predictive of improvements in depression symptoms[59]. Involvement of alterations in both innate and adaptive immune systems in MDD and treatment response has been well established[62–64], although exact mechanisms remain elusive. The role of p11 in MDD should be further investigated, as well as its possible role as a biomarker to detect treatment response.

1.4 KETAMINE

Ketamine, an N-methyl-D-aspartate (NMDA) receptor antagonist, was first developed for its anesthetic and analgesic properties[65]. However, studies from the last two decades showed ketamine's potential to act as an antidepressant with long-lasting effects in patients with treatment-resistant depression[7,66–68]. Unlike the slow onset of common antidepressants, ketamine has shown to induce a rapid antidepressant effect within hours[7,68], while a single administration showed to be effective for a week[68].

Ketamine has historically been administered intravenously, but recently the American Food and Drug Administration approved the more patient-friendly S-ketamine nasal spray for treatment of treatment-resistant depression in adults, to be used in combination with an oral antidepressant. The clinical application of ketamine is still restricted due to its numerous side effects, including dissociative effects, loss of appetite, hallucinations and abuse liability[8]. Moreover, long term administration of ketamine has been suggested to induce cognitive deficits in humans and is associated with cell apoptosis in the prefrontal cortex of non-human primates[69,70]. Development of fast and effective MDD treatments, with less undesirable effects, may benefit from knowledge on the effects of ketamine. However, the antidepressant mechanism of action of ketamine remains largely unknown.

Research on the antidepressant properties of ketamine has mostly been focused on the glutamate system[2]. The antidepressant action of ketamine was found to be dependent on the glutamate α-amino-3-hydroxy-5-methylisoxazole-4-propionic acid (AMPA) receptor[71,72]. Ketamine produces presynaptic glutamate release, and is suggested to exert its rapid effect by an increased activation of AMPA relative to NMDA receptors, which may activate neuroplasticity systems[71,72] (Figure 2).

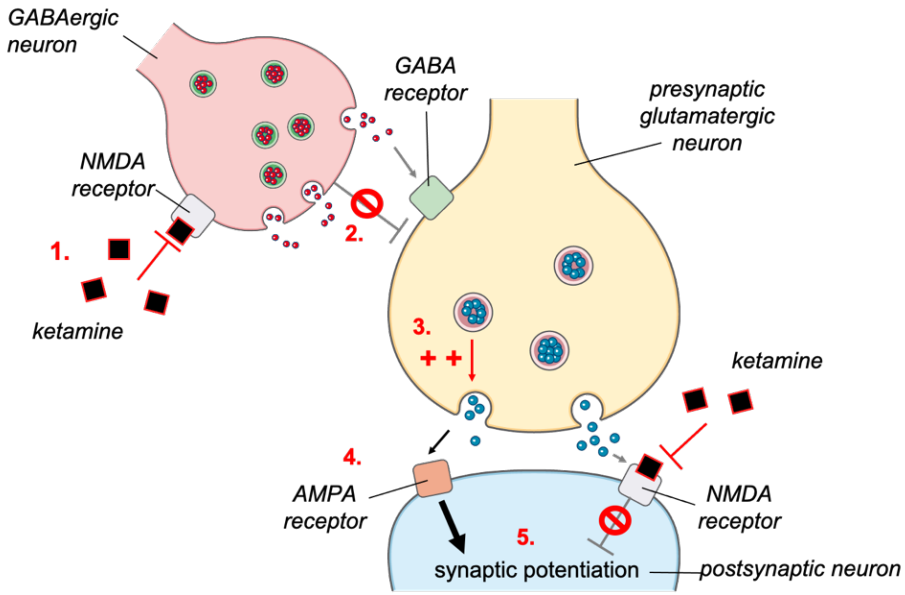

Figure 2: Schematic representation of a suggested antidepressant mechanism of action of ketamine. 1: Ketamine blocks NMDA-receptors, including those on GABAergic interneurons; 2. Inhibition of GABA release causes disinhibition of the glutamatergic neuron; 3. Glutamate is more excessively released; 4. Glutamate binds towards the AMPA-receptor on the postsynaptic neuron and is prevented from binding to NMDA-receptors by ketamine; 5. The increased glutamate AMPA vs NMDA throughput induces synaptic potentiation.[71,72] Figure created by using images from Servier Medical Art (http://smart.servier.com/), licensed under CC BY 3.0

Ketamine also has strong effects on other mechanisms than NMDA inhibition: affinity has been shown towards opioid, muscarinic, nicotinic and serotonergic receptors[73]. A role for the serotonin system has been proposed in the antidepressant action of ketamine[74]. Serotonin depletion in rodent model of depression was shown to diminish the antidepressant effect of ketamine, which could be restored with a 5-HT_{1B} receptor agonist[75]. In a non-human primate PET study, administration of ketamine increased the availability of 5-HT_{1B} receptors in the ventral striatum, which was dependent on activation of the AMPA receptor[76]. Also, protein p11 was demonstrated to play a role in the sustained antidepressant effect of ketamine in the hippocampus of an animal model of depression[77], although the exact mechanism remains unclear.

1.5 AUTORADIOGRAPHY

1.5.1 Principles of Autoradiography

The word autoradiography is derived from the Latin and Greek words *auto* (= self), *radius* (=ray) and *graphein* (to write); i.e. the studied object itself is the source of radiation. With this technique, an image is created from the pattern of decay emission on a film or emulsion. Due to the high sensitivity and high resolution of this technique, autoradiography can be used to localize and quantify radioligand binding[78]. ARG may provide an indication on whether a radioligand is suitable for *in vivo* PET, especially with regards to affinity, selectivity and non-specific binding.

In a typical *in vitro* ARG procedure, a sample (slice, tissue homogenate or cells from a cell culture) is incubated with radioligand solution, after which the sample is washed, dried and then placed in direct contact with either radiosensitive film, photostimulable phosphor plate or photographic emulsion. For the quantitative ARG experiments in this thesis, a ^{3}H-labeled ligand and photostimulable phosphor films are used, together with calibrated radioactive samples. Upon decay of this radioisotope, a β-particle (electron) is emitted, which can excite electrons in the phosphor film. When the film is exposed to helium/neon laser light, the excited electrons go back to their ground state and a photon is released. These photons are recorded by a photomultiplier tube. The result is a record of localized light intensity, which is proportional to the amount of ionizing radiation. With the calibrated samples, this signal can be transformed into apparent binding densities.

High resolution ARG, as also used in study I, is applicable when information regarding cellular location of the bound radioligand is required. The tissue sections are coated in photographic emulsion. This emulsion contains silver halides, which react to the beta particle decay, leaving silver grains. This results in a higher resolution radioligand signal, which can be studied by microscope.

1.5.2 Ligand-receptor interaction

A common application for ARG is to study the properties and interactions of a PET radioligand with its target. ARG enables the direct measurement of specific binding, the assessment of the affinity of the interaction and rate constants for the ligand-target interaction. This application

is complementary to *in vivo* PET and important for a direct comparison with *in vivo* brain images[79]. Using ARG, these properties can be studied *in vitro* on *post mortem* tissue in a controlled lab environment.

Specificity towards the target can be directly measured using ARG by a competitive-binding assay: comparing radioligand binding with addition of excess cold ligand (not labeled with a radioactive isotope). When a cold ligand is used with known high specificity towards the same target, the resulting binding can give an indication of non-specific binding (Figure 3). Specific binding densities within the sample can then be calculated by subtracting the non-specific binding from total binding (i.e. radioligand binding without blocking with cold ligand). Administration of excess ligand *in vivo* could result in a pharmacological response and is therefore not desired.

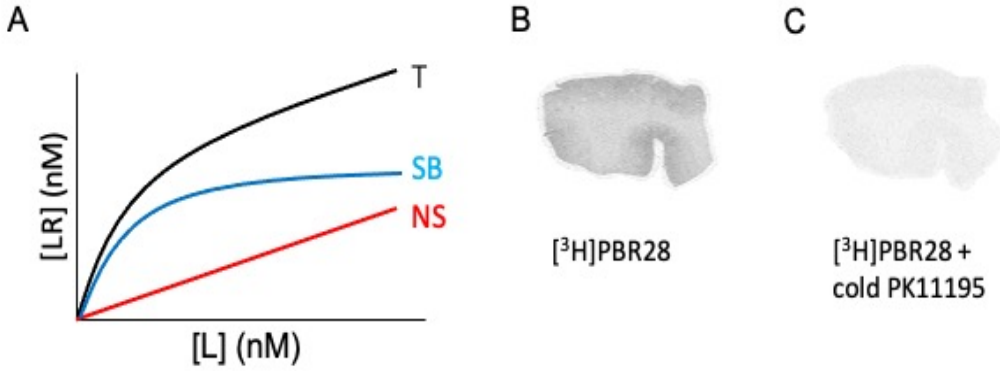

Figure 3: A) Concentration of ligand [L] plotted against concentration bound ligand to receptor [LR] for total binding (T), non-specific binding (NS) and specific binding (SB). B) Total binding of the radioligand [^{3}H]PBR28 in the frontal lobe of a healthy subject. C) Consecutive slice of B, showing binding of [^{3}H]PBR28 and blocking by excess PK11195, representing non-specific binding

In vitro binding of ligand L to receptor R can be described schematically by equation 1.1, a derivation of a model proposed by Michaelis Menten for enzyme binding to a substrate. The rate constants of the forward and backward reaction of ligand binding to the receptor are k_{on} and k_{off} respectively. This equation shows that the rate at which binding of the ligand to the receptor occurs, is proportional to the concentration of ligand and receptor. Similarly, the dissociation rate is proportional to the concentration of bound receptor. In order to get a reproducible outcome measure, the concentration of bound receptor is measured after enough time has been allowed for the rate of association to be equal to the rate of dissociation, i.e. the reaction has reached equilibrium.

$$[L] + [R] \underset{k_{off}}{\overset{k_{on}}{\rightleftarrows}} [LR] \qquad 1.1$$

As with enzyme kinetics, the receptor-ligand interaction reaches a plateau due to saturation of the receptor. For ARG quantification of receptor densities, radioligand concentrations approach saturation of the target (B_{max}: total receptor density). This can be visualized by the saturation curve as shown in Figure 4 and is described by equation 1.2, a derivation of the Michaelis-

Menten equation. When the concentration of free ligand equals K_d, the equilibrium dissociation constant, half of the maximum concentration of available receptors is bound. K_d is the ratio of the rate constants k_{off} and k_{on}. The reciprocal of K_d represents the affinity of the ligand towards the receptor. For radioligands, K_d typically describes concentrations in the nanomolar (nM) level.

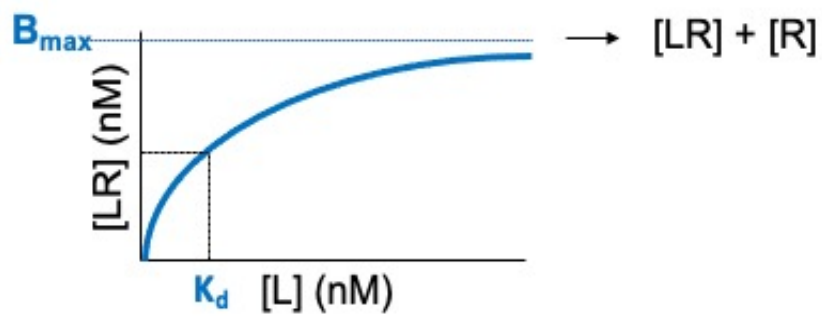

Figure 4: Saturation-binding curve: Concentration of ligand [L] plotted against concentration ligand specifically bound to receptor [LR]. The asymptote of the curve is B_{max}, the maximum concentration of receptors in the sample. When [L] = K_d, the equilibrium dissociation constant, half of B_{max} is bound.

$$[LR] = \frac{B_{max} * [L]}{K_d + [L]} \qquad 1.2$$

1.5.3 Resolution: ARG vs PET

An advantage of ARG over PET is its relatively high spatial resolution. The resolution in ARG is < 0.1 mm[80], while in PET, even when using the high-resolution research tomograph (HRRT) a resolution of 1.5 mm can be achieved[81,82]. This can partly be explained by the fact that radioisotopes suitable for ARG can have much lower energy (e.g ^{3}H, energy: 6 keV) than radioisotopes suitable for PET (e.g. ^{11}C, energy: 967 keV) [83]. Lower radioactive energy beta-particles travel a smaller distance from the source and therefore divert less from their original position. Moreover, detection of radiation at close proximity to the tissue also reduces the limiting effects of scatter on resolution. Radiation can be attenuated and scattered upon interaction with matter. The larger the distance between object and detector, the more the resolution will be negatively affected by scatter. Further factors determining resolution in PET are discussed in the next chapter.

1.6 POSITRON EMISSION TOMOGRAPHY

1.6.1 Application

PET is a non-invasive imaging technique that can provide functional information of the brain *in vivo*. It has a high sensitivity and specificity, enabling visualization and quantification of biochemical and metabolic processes. PET can facilitate drug discovery in microdosing, occupancy and biomarker studies[84]. In microdosing studies, a drug candidate is labeled with a radioactive isotope. This enables the examination of the uptake and distribution of the drug

throughout the body and therefore also enables the assessment of penetration of the blood-brain barrier (BBB). In occupancy studies, radioligand binding is studied before and after administration of a drug. In this way, the receptor population occupied by the drug can be defined. This can be useful to investigate whether the target is engaged in the working mechanism of the drug[85] or to guide drug dose selection[86]. In biomarker studies, target proteins can be studied in relation to pathophysiology, disease progression, monitoring treatment effect and studying the mechanism of a drug. The most common application in clinical practice for PET is the use of a biomarker for glucose metabolism in cancer: ^{18}F-FDG (fluorodeoxyglucose)[87], to measure localized increases of glucose utilization. In the CNS, PET radioligands are, among others, used to examine β-amyloid load, a biomarker used for diagnosis of Alzheimer's disease[88]. Although several biomarkers have been proposed for psychiatric disorders, there is currently no consensus for their use in clinical practice.

1.6.2 Radioligand

The high specificity of PET is dependent on the use of specific ligands labeled with a radioactive isotope (a radionuclide). Common ligands for use in PET are radiolabeled with a short-lived nuclide, such as ^{11}C (half-life = 20.3 min), which is also used for the radioligand applied in this thesis. Radionuclides with a longer half-life, such as ^{18}F (half-life = 110 min) are needed in case there is no cyclotron to produce the radionuclide and a radiochemistry facility at the study site. Radioligands should have high affinity and high selectivity for the target, while showing low non-specific binding. Furthermore, PET ligands suitable for CNS imaging are designed taking into account the pharmacokinetic properties shown in Table 1[84,89].

Table 1: Criteria of PET ligands in relation to pharmacokinetics

Pharmacokinetic parameter	Key Criteria
Absorption (through BBB)	Allow passive diffusion through BBB, e.g. size: < 500 Da, < 80Å^2, lipophilicity: partition coefficient (log P): +1 to +4
	Not a substrate for P-glycoproteins (efflux transporter)
	Limited penetration of metabolites through BBB
Distribution	Low (pharmacological) volume of distribution
	Low plasma protein binding
	Limited accumulation in peripheral tissue compartments
Metabolism	Limited peripheral metabolism
	No central metabolism
Elimination	Rate: enable observation of washout for kinetic analysis

BBB: blood brain barrier

The produced radioligand should enable administration of a low injected mass. In that case, the proportion of unlabeled ligand is low, which minimizes the competition with the binding of labeled ligand towards the target. Moreover, the labeled ligand concentration should be sufficient to be detected by the PET system. This is represented by a high *molar activity*: the ratio of injected radioactivity to the number of moles of radioligand.

1.6.3 Measurement

During the PET examination, the radioligand is commonly administered through venous injection. The radioligand is then distributed throughout the body via the blood stream after which it can bind to the target of interest. Radionuclides used in PET are β^+-emitters, i.e. they emit positrons upon decay. This positron will travel a short distance, called the *positron range*[90], before it collides with an electron. The positron range is positively correlated to the energy of the radionuclide; for ^{11}C, the positron range is about 1 mm[90]. The collision of a positron and an electron induces annihilation, which induces the emission of two γ-photons in approximately opposite directions (Figure 5). The fact that these photons do not travel exact opposite directions is called the *photon non-collinearity effect*[91]. The photons are detected by the PET system, which contains a ring of detectors around the study subject. When two photons are detected within a certain timeframe, it will be recorded as a coincidence event. Together, these two detected photons provide positional information on where the annihilation has taken place: they are assumed to originate from a point at the line of response between the two detectors.

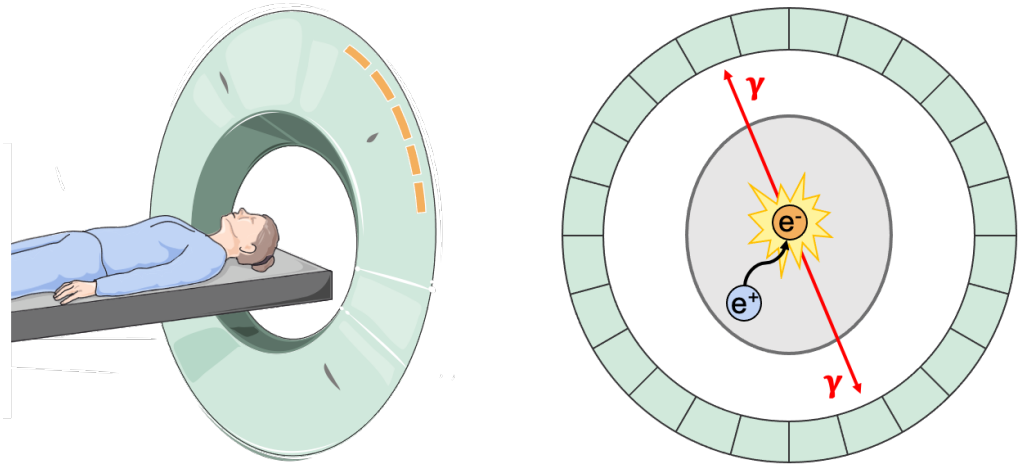

Figure 5: Schematic representation of signal detection in the PET system. Right: A collision of a positron (blue) with an electron (orange) results in annihilation, after which two γ-photons are emitted towards approximately opposite directions. The γ-photons detected within a short time frame are recorded as a line of response (red line) between two detectors. It is assumed that somewhere along this line of response the annihilation took place. Part of the figure is created by adapting images from Servier Medical Art (http://smart.servier.com/), licensed under CC BY 3.0

After collection of all the coincidence events during a PET examination, a 3D representation of the radioactivity distribution is reconstructed. Many photons are however also detected as coincidence events, while they actually originate from two different annihilations ('random events') or from scatter. The detection of these erroneous line of responses are to a large degree corrected for by the reconstruction process, which limits resolution loss and noise in the data. Other factors influencing the resolution include: the size and material of the used detectors[92], the positron range (annihilation does not take place at the exact location where the radioligand decayed) and the photon non-collinearity effect. The resolution limitation in PET leads to areas with spill-over and spill-in of signal originating from nearby areas, called the *partial volume effect* (PVE)[93]. Resolution in PET systems is being improved by technological developments

in detection systems[94] and the application of more advanced reconstruction methods[82]. The impact of photon non-collinearity and scatter on resolution is reduced in PET systems designed for brain imaging compared to whole body PET, by decreasing the diameter of the ring of detectors.

1.6.4 Quantification

Ligand binding can be quantified per voxel (3D pixel) or as average in all voxels in a volume of interest (VOI). In order to define regions of interest PET, PET is ideally complemented by a modality which can provide anatomical information. Commonly, Magnetic Resonance Imaging (MRI) is used for this purpose. MRI provides information on proton densities, e.g. cerebral gray and white matter can be differentiated on MR images due to differences in the concentration of H_2O, which is rich in protons. The MR image is co-registered to the PET image to enable the measurement of radioactivity in a VOI.

In this thesis, 3D dynamic PET data is acquired, i.e. a series of 3D PET images are acquired during multiple time frames. When plotting the radioactivity concentration of each time frame within each voxel or VOI, a *time activity curve* (TAC) is obtained. In contrast to ARG, there is no option to directly measure the concentration of specifically bound ligand to the receptor for quantification with PET. Instead, measured radioactivity is normalized to a reference factor as an estimate of specific binding. In clinical practice, the Standard Uptake Value (SUV) is used. To calculate the SUV, measured radioactivity concentration at a predefined time is normalized by the injected dose divided by the body weight of the study subject. However, the validity of this outcome measure is strongly affected by noise, image resolution and definition of the region of interest[95]. In biomedical research, more robust outcome measures are desired. For the PET studies in this thesis, binding potential is used as outcome measure, which is defined as the ratio of B_{max} (total receptor density, see section 1.5.2) to K_d (radioligand equilibrium dissociation constant)[96]. This means that binding potential is both dependent on receptor densities and the affinity of the ligand for the receptor. It is generally assumed that affinity does not differ between study subjects or brain regions, hence differences in binding potential reflect differences in receptor concentrations[97].

For a comparison of the *in vivo* outcome measure binding potential with the *in vitro* outcome measure specific binding, equation 1.2 (regarding *in vitro* receptor ligand binding) can be redefined to *in vivo* terms, where concentration of bound receptor [LR] = B and concentration of free ligand [L] = F:

$$B = \frac{B_{max} * F}{K_d + F} \qquad 1.3$$

During *in vivo* PET measurements, receptor binding does not approach saturation. Instead, only a tracer dose of the radioligand is used, often occupying <5% of available receptors[96]. This prevents the occurrence of a pharmacological response, which would influence the *in vivo* system and could affect the study subject. In this way, injected radioactivity can be kept to a minimum even with high molar activity and low injected mass. Tracer dose conditions are used

to derive a robust outcome measure, which can be explained as follows: for *in vivo* PET, the concentration of F will be much lower than K_d and equation 1.3 can be rearranged to:

$$B = \frac{B_{max} * F}{K_d} \rightarrow \frac{B}{F} = \frac{B_{max}}{K_d} \qquad 1.4$$

Therefore, at tracer dose conditions, binding potential can also be described as the concentration of bound ligand to concentration of free ligand. Then, the ratio of the concentration of bound ligand to free ligand is a constant. This is visualized in the plot displayed in Figure 6, similar to the saturation curve described for *in vitro* binding (Figure 4). When the concentration of bound and free radioligand are very low, the slope is linear: if the concentration of free ligand increases, the concentration of bound linear increases proportionally. Small differences in injected radioligand therefore do not affect binding potential. Note that even though only a small proportion of the receptors are occupied at tracer doses, binding potential represents binding of the total amount of receptors.

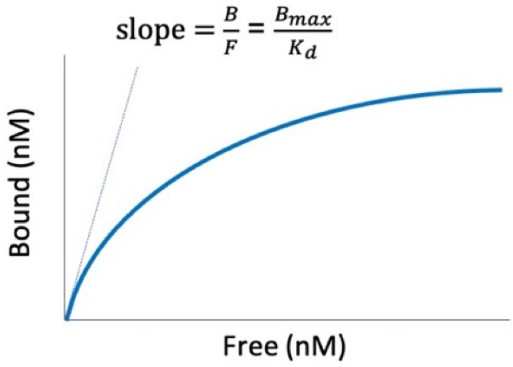

Figure 6: Saturation-binding curve: the concentration of free radioligand (F) plotted against the concentration of bound radioligand to the receptor (B). The initial slope of the curve is linear. At tracer dose conditions, B and F are low and the slope of the curve $\frac{B}{F} = \frac{B_{max}}{K_d}$ (equation 1.4).

In order to measure the binding potential in the VOI or voxel, a kinetic model is used. As mentioned earlier, instead of measuring specific binding directly, when using *in vivo* PET, measured radioactivity is normalized to a reference factor. This reference factor can for example be radioactivity concentration measured in arterial plasma, or as used in this thesis: radioactivity concentration in a reference region in the brain which contains negligible amounts of the target. The model should describe the TAC and the behavior of radioligand binding in the tissue region of interest and in the reference region. Commonly, compartmental models are used for this purpose. These compartments represent the different physical locations (e.g. brain tissue, blood) or states (e.g. bound, free) in which the radioligand transfers and contains a homogeneous tracer concentration. As the behavior of different radioligands can differ, they might also be better described with different number of compartments and rate constants between compartments[98,99].

The basis for most compartmental models to describe radioligand binding in PET is the three tissue compartment model (Figure 7A). This model describes the transfer of radioligand concentration from plasma (C_P) to free ligand in target tissue (C_F) and vice versa, with rate constants K1 and k2 respectively; transfer of radioligand from C_F to specifically bound ligand (C_S) and vice versa, with rate constants k3 and k4 respectively; and transfer of radioligand from C_F to non-specific binding (C_{NS}) and vice versa, with rate constants k5 and k6 respectively. When the transfer between the compartment with non-specific binding and the one with free tracer is assumed to be sufficiently fast, both can be collapsed into one compartment containing non-displaceable binding (C_{ND}).

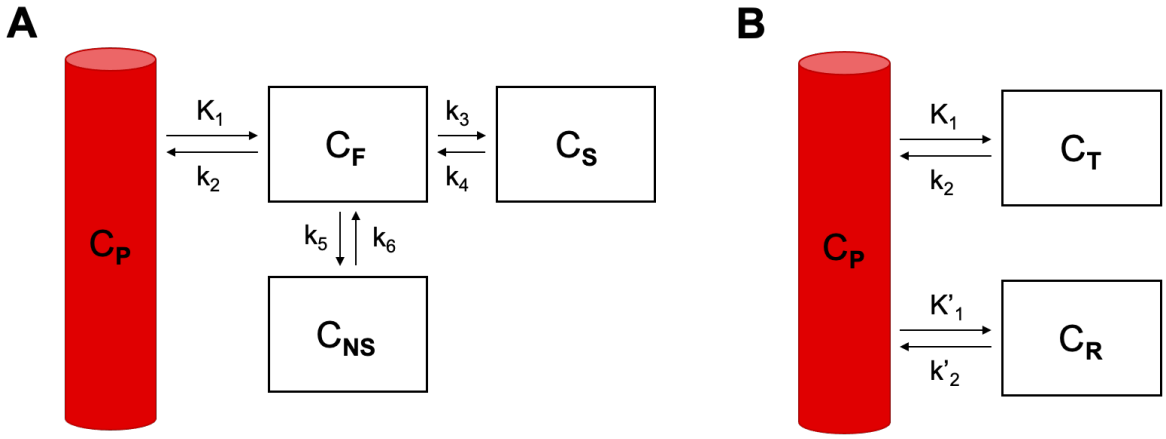

Figure 7: A) Three tissue compartment model. Boxes represent compartments describing radioligand concentration in: plasma (C_P), free ligand in target tissue (C_F), specifically bound ligand (C_S) and non-specifically bound ligand (C_{NS}).
B) Simplified Reference Tissue Model, with compartments describing total radioligand concentration in target tissue (C_T) and reference tissue (C_R).

TACs from the radioligand used in this thesis have been shown to be well described[28] by the Simplified Reference Tissue Model (SRTM)[100] (Figure 7B). Rate transfer between C_{NS} and C_F are considered sufficiently fast to collapse into one C_{ND} compartment. Furthermore, this model uses a brain tissue region as reference, assumed to contain no specific binding. The compartment for the reference region (C_R) therefore only contains one compartment with C_{ND}. In the target tissue, the rate of transfer between C_{ND} and C_S is considered to be sufficiently fast enabling the possibility of these two compartments to be collapsed into one total tissue concentration compartment (C_T). The rate constants for transfer from and to C_P and C_T are K1 and k2, respectively; for transfer from and to C_P and C_R the rate constants are K'1 and k'2, respectively. It is not possible to separately derive K1 and K'1, instead this is derived as the ratio $R1 = \frac{K1}{K'1}$ C_{ND} is assumed to be the same in the target and the reference region, therefore:

$$\frac{K1}{k2} = \frac{K'1}{k'2} \rightarrow k'2 = \frac{k2\,K'1}{K1} = \frac{k2}{R1} \qquad 1.5$$

which results in three parameters to be estimated: R1, k2 and the outcome measure non-displaceable binding potential (BP_{ND}). BP_{ND} is defined as the ratio of specific concentration to

non-displaceable concentration at equilibrium and can be determined as follows:

$$BP_{ND} = \frac{C_T - C_R}{C_R} \qquad 1.6$$

where C_T represents total radioligand concentration in target tissue and C_R the total concentration in reference tissue. The *in vitro* analogue of this would be[96]:

$$BP_{ND} = \frac{f_{ND} * B_{avail}}{K_d} \qquad 1.7$$

where f_{ND} represents the free fraction of ligand in the non-displaceable compartment and B_{avail} is the concentration of receptors available for measurement *in vivo* (as opposed to B_{max} in ARG, where all receptors are theoretically available for the radioligand to be bound). When assuming that f_{ND} does not differ between study subjects, just like is assumed for K_d, BP_{ND} represents an estimation of the densities of available receptors in the target region.

1.6.5 Imaging the 5-HT$_{1B}$ receptor

In PET imaging studies focusing on 5-HT$_{1B}$ receptor densities, currently two ligands are being used: [^{11}C]P943[101] and [^{11}C]AZ10419369[102]. Both radioligands have shown good test-retest reliability[103,104]. Although no direct comparison has been made so far, [^{11}C]AZ10419369 has shown to result in higher affinity[105] and BP_{ND} in human subjects[28,106], which could reflect a higher signal-to-noise ratio. Both [^{11}C]AZ10419369[107–109] and [^{11}C]P943[110,111] have been shown to be sensitive to pharmacologically induced changes of endogenous serotonin levels. [^{11}C]AZ10419369 PET is selective for the 5-HT$_{1B}$ receptor with high binding in the 5-HT$_{1B}$ rich cortical regions[28,102] and low binding in the cerebellum[28,102], a region known to be nearly devoid of 5-HT$_{1B}$ receptors[112,113]. AZ10419369 acts a partial agonist for the 5-HT$_{1B}$ receptor[105], i.e. although it fully binds to the receptor, it does not induce a full pharmacological effect.

Although test-retest reliability of quantification with [^{11}C]AZ10419369 has been shown to be good in cortical regions and acceptable in subcortical regions, high variability of 5-HT$_{1B}$ receptor density measures has been seen in the dorsal part of the midbrain[104]. The relatively low reliability for quantification in the brainstem is likely caused by the poor visibility of small brainstem nuclei on MRI, therefore requiring an alternative approach for delineation of a VOI. Previously, methods have been reported to improve 5-HTT density quantification in brainstem nuclei[114,115]. Whether these methods are applicable for 5-HT$_{1B}$ receptor density quantification is uncertain, as the 5-HT$_{1B}$ receptor has *in vitro* been shown to possess a different distribution pattern and receptor density[113]. For example, in the substantia nigra and the central gray area, high 5-HT$_{1B}$ receptor densities were found[112,116], while in the dorsal raphe nuclei, 5-HTT receptors were more abundant[113]. This difference in localization is likely to be explained by their functional differences: while 5-HTT are only located on serotonergic neurons, 5-HT$_{1B}$ receptors can also function as heteroreceptors on other neuron types[25]. Therefore, 5-HTT binding quantification methods have to be tested for application in PET studies on the 5-HT$_{1B}$ receptor.

2 RESEARCH AIMS

The overall objective of this thesis was to study cerebral 5-HT_{1B} receptor densities and peripheral p11 protein levels in MDD patients in relation to treatment with ketamine. The specific aims were to investigate:

Study I: The *in vitro* ARG distribution of 5-HT_{1B} receptor densities in the anterior cingulate cortex at high resolution and to investigate if 5-HT_{1B} receptor densities in MDD subjects could be differentiated from those in subjects with schizophrenia, bipolar disorder and healthy subjects.

Study II: The *in vitro* ARG distribution of 5-HT_{1B} receptor densities in brainstem tissue from a healthy subject and to use this information to improve a quantification method of 5-HT_{1B} receptor availabilities in the brainstem using PET.

Study III: The effect of ketamine treatment in SSRI-resistant MDD subjects on 5-HT_{1B} receptor availability using PET, in relation to treatment response.

Study IV: The effect of ketamine treatment in SSRI-resistant MDD subjects on p11 levels in peripheral blood using Flow Cytometry. As in study III, this effect is studied in relation to treatment response to examine the possibility that peripheral p11 could serve as a biomarker of antidepressant response of ketamine in MDD patients.

3 MATERIALS AND METHODS

3.1 ETHICAL CONSIDERATIONS

All studies were approved by the Ethics Committee of the Stockholm Region. Additionally, study II was also approved by the Semmelweis University Human Ethical Committee and study III was approved by the Radiation Safety Committee of the Karolinska University Hospital. Study I and II contain *post mortem* tissue from anonymous donors. For study II-IV, subjects gave their written and verbal consent before initiation of study procedures. For study III-IV, patients were carefully informed about the risks of withdrawing medications. Personal data was carefully stored at a secure network and acronyms were used during analysis.

Study III was carried out double-blind and analysis of the PET data was also carried out blinded to treatment allocation. Furthermore, the analysis protocol of this study was pre-registered, including for example the VOIs to be analyzed.

3.2 AUTORADIOGRAPHY (STUDY I-II)

3.2.1 *Post mortem* brain tissue

None of the donors had known history or symptoms of neurological or psychiatric disorders (except for those studied in study I) and none of the brains exhibited damages or abnormalities from examination at autopsy and during sectioning.

Study I: Human *post mortem* brain tissue was obtained from the Stanley Foundation, Bethesda, USA, who collected brains with family permission. Tissue originated from the ACC from the Neuropathology Consortium brain collection[117], of which the present project had access to the following subset: brain slices derived of 52 individuals between 25 and 68 years old, of which 14 diagnosed with bipolar disorder, 12 with MDD, 13 with schizophrenia and 13 healthy control subjects (the original collection consisted of material of 15 subjects of each group). The key to medical relevant information (such as diagnosis and age) was provided after data was sent to the Stanley Foundation.

Study II: Human brain tissue (Table 2) was obtained *post mortem* at clinical autopsy at the Department of Forensic and Insurance Medicine, Semmelweis Medical University (Budapest, Hungary); the National Institute of Forensic Medicine, Karolinska Institutet (Stockholm, Sweden) and at the Human Brain Tissue Bank (Budapest, Hungary).

Table 2: Demographic and clinical specifications of donated brain tissue for study II

Region	Age (y)	Sex	PMI (h)	Cause of death
Hemisphere	54	M	22-23	Coronary heart disease
Hemisphere (L)	59	F	11	Cardiac failure in septic state
Hemisphere (L)	63	M	48	Myocardial infarction
Brainstem (R)	68	M	< 24	Right ventricle failure
Brainstem	34	F	< 24	Thrombotic occlusion of pulmonary arteries

PMI: *post mortem* interval

3.2.2 Compounds

The radioligand [^{3}H]AZ10419369[102] (Figure 8) was used for the ARG experiments of study I and II. [^{3}H]AZ10419369 has shown high specificity and affinity for a single binding site on human 5-HT$_{1B}$ receptors[118], which makes this radioligand highly suitable for studying the 5-HT$_{1B}$ ligand in detail. [^{3}H]AZ10419369 was synthesized at Karolinska Institutet, department of Clinical Neuroscience (study I) and purchased from Novandi Chemistry AB (Södertälje, Sweden; study II). Molar activity was 21 Ci/mmol and 83 Ci/mmol, respectively. Radiochemical purity was >98%. Kodak NTB emulsion was purchased from VWR, Sweden.

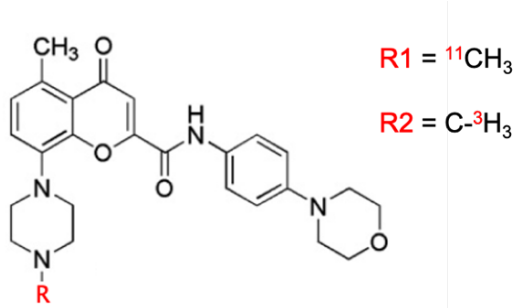

Figure 8: The serotonin 1B binding ligand AZ10419369, labeled with either ^{11}C (R1) for use with the PET studies (study II & III) or with ^{3}H (R2) for use with the ARG studies (study I & II) in this thesis

3.2.3 Cryosectioning

Fresh frozen *post mortem* tissue was sectioned on a cryomicrotome (Leica CM 1860 Leica, Nussloch, Germany) or heavy-duty cryomicrotome (Leica cryomacrocut CM3600), thaw mounted to poly-l-lysine-treated or gelatinized glass plates, dried at room temperature and stored according to the specifications in Table 3.

Table 3: Specifications for cryostat procedure

	Region	Plane	Slice thickness	Storage temperature
Study I	ACC	Axial	14 µm	-70°C
Study II	Hemisphere	Axial: 3-4 levels	100 µm	-25 °C
	Brainstem	Sagittal & Axial	20µm	-20 °C

In study II, the sagittal brainstem slides were sectioned leaving 0.5 mm of tissue between each consecutive slide. Photographic images of the frozen tissue were digitally recorded before cutting of each section and at the end of the cryostat wheel crank course, as previously described[119].

3.2.4 [^{3}H]AZ10419369 *in vitro* autoradiography

Sections were incubated at room temperature for 60 minutes in 1.5 nM [^{3}H]AZ10419369 in buffer containing Tris-HCl 50 mM, pH 7.4 incl. 4 mM MgCl, 4 mM $CaCl_2$. In study II, 0.1% bovine serum albumin was added to the incubation buffer to decrease non-specific binding, e.g. to the tissue embedding material carboxymethyl cellulose, which was not used in study I. Adjacent sections were simultaneously incubated in the previously mentioned buffer with addition of 10 µM 5-HT. After washing and drying, sections were placed together with

autoradiographic micro-scale standards (American Radiolabeled Chemicals Inc.), and exposed to phosphor imaging plates (Fujifilm Plate BAS-TR2025, Fujifilm, Tokyo, Japan) for four days. Image radioactivity was detected using a Fujifilm BAS-5000 phosphor imager (Fujifilm, Tokyo, Japan), which resulted in scanned images with signal representing average photostimulated luminescence (PSL)/mm^2.

3.2.5 High resolution autoradiography (study I)

High resolution microscopic emulsion ARG was performed in order to visualize the cellular distribution of the radioligand in the ACC. Slices were dipped into NTB emulsion at 42°C, air-dried at room temperature and exposed in the dark at 4°C for 3-4 weeks. Slides were then developed with Dokumol developer, rinsed in water, fixed with Vario Fix in room temperature and washed with water.

3.2.6 Nissl staining

Nissl staining was performed to provide anatomical information and guide definition of Regions of Interest (ROIs). Slides were stained with cresyl violet (Histolab, Göteborg, Sweden), dehydrated consecutively in increasing concentrations of ethanol, immersed in Histolab Clear (xylene substitution, Histolab, Göteborg, Sweden), dried and mounted.

3.2.7 Defining regions of interest

Guided by Nissl-staining, gray matter ROIs were manually drawn using Multi Gauge 3.2 phosphor imager software (Fujifilm, Tokyo, Japan). Using the processed micro-scale standards, mean PSL/mm^2 of each ROI was transformed into radioactivity values and binding density (pmol/mg tissue wet weight). Specific binding was determined by subtracting the level of non-specific binding from the total binding.

3.2.8 Volume rendering (study II)

Image preprocessing was performed using Fiji/ImageJ[120] version 1.50i. Photographic images taken during cryosectioning were used as a reference volume for the processed ARG and Nissl-stained brainstem sections, to control for possible sectioning related deformations[121]. First the photographic images were aligned and stacked. Then the ARG binding slices were co-registered section-to-section to the photographic volume, using the Nissl-stained slices as intermedial modality. Subsequently, an ARG specific binding stack was generated by subtracting the information of the non-specific binding slices from the total binding slices, after which the stack was mirrored to represent ARG binding in a complete brainstem.

The ARG brainstem volume was transformed into the standard reference space of the Montréal Neurological Institute (MNI[122]). This was performed by first using an affine transformation towards a substantia nigra weighted brainstem and subsequently applying a non-linear registration.

ARG images of [^{3}H]AZ10419369 on axial slices were used to confirm binding localization visually in the axial plane.

3.3 POSITRON EMISSION TOMOGRAPHY (STUDY II-III)

3.3.1 Study subjects

Health of the subjects (study III: excl. their MDD) was confirmed by medical history and physical examination, including routine blood tests and MRI of the brain.

Study II: This study included data from 60 healthy subjects, of which 52 were pooled and used to create a database. This includes data from 33 subjects of which results were previously published in PET-studies[107,123–125]. Furthermore, 8 subjects were part of a test-retest study[104] and were in this study used for testing purposes in this study. The database consisted of 32 male and 20 female subjects, 38.2 ± 17.9 years of age (mean ± SD); the testing subjects were all male and 23.0 ± 2.3 years of age.

Study III: Patients were recruited through internet-based advertisement. Patients had an ongoing MDD episode according to Mini International Neuropsychiatric Interview[126], with MADRS[126] score of ≥20 and were treated for at least four weeks with an SSRI in adequate doses without treatment response. Patients were randomly allocated to either active treatment with ketamine (n=20; 8 females; age = 39.2 ± 11.6 years; baseline MADRS = 26.3 ± 6.6) or placebo treatment (n=10; 6 females; age = 37.1 ± 11.2; baseline MADRS = 30.8 ± 4.9).

3.3.2 Treatment protocol (study III)

An antidepressant washout period of at least 5 drug half-lives was carried out prior to initiation of the examinations. At baseline, MADRS scores were assessed, venous blood samples were collected and the first PET examination was carried out. Within 2 days subjects were administered study treatment (double-blind, either active treatment with 0.5 mg/kg racemic ketamine diluted in 100 mL isotonic NaCl solution or placebo treatment with 100 mL isotonic NaCl solution) as one intravenous infusion for 40 minutes. A second MADRS assessment, blood sample withdrawal and PET examination were carried out 1-2 days after treatment. Subsequently, subjects in both groups were treated with open-label ketamine in 2-4 occasions within 2 weeks, after which a final MADRS assessment was performed.

As the MDD symptoms insomnia and loss of appetite are also reported side effect of ketamine[8], calculations on changes in symptom severity were based on an adjusted MADRS in which these two factors were left out, resulting in an 8-item MADRS, as preregistered at Aspredicted.org (#17602).

3.3.3 PET examinations

[^{11}C]AZ10419369 (Figure 8) was synthesized as previously described[102]. All PET examinations were performed using the HRRT (Siemens Molecular Imaging, Knoxville, USA). A bolus injection of [^{11}C]AZ10419369 was administered after which the intravenous line was flushed with saline. To minimize head motion during the PET examination, an individually made plaster helmet was used. Emission data was acquired in list mode for 63 to 95 min and dynamic images were reconstructed in a series of 32-38 time frames using 3D ordinary Poisson ordered subset expectation maximization, including modeling of the system's point spread function. This reconstruction protocol has previously been shown to provide a

resolution of approximately 1.5 mm full width half maximum in the center of the field of view and 2.4 mm at 10 cm away from the center[82].

3.3.4 MRI examinations and analysis

T1-weighted MR images were acquired on a 3T GE MR750 scanner (GE Medical Systems, Milwaukee, WI; study II & III) and a 1.5T GE Signa (GE Medical Systems, Milwaukee, WI) or 1.5T Magnetom Avanto (Siemens Medical Solutions, PA, USA; study II: two subjects in database). These MR images were co-registered with PET images and segmented into gray matter, white matter and cerebrospinal fluid using SPM12. Furthermore, inverted co-registration parameters were obtained to transform VOIs from MR to PET space. VOIs outside the brainstem were defined using Freesurfer (5.0.0, http://surfer.nmr.mgh.harvard.edu/).

3.3.5 PET image analysis

Images were corrected for head motion with a post-reconstruction frame-to-frame correction realignment algorithm as previously described[127], and in the case of excessive head motion, with an additional motion correction algorithm based on the simplex method[128]. All PET data underwent minor motion correction using a frame-by-frame correction algorithm from SPM12.

For VOIs outside the brainstem, BP_{ND} was calculated using SRTM, with the cerebellum as reference region. For analysis of VOIs in brainstem, a wavelet-aided parametric imaging (WAPI) algorithm[129] was used to create parametric BP_{ND} images. This approach uses a reiterative wavelet-based denoising method and the non-invasive Logan plot fitted by multilinear regression to calculate BP_{ND} in each voxel. This method overcomes the VOI-size limitation of VOI-based compartment modeling and can therefore be used to quantify small brainstem regions. For study III, regional BP_{ND} values in the dorsal brainstem were calculated using the [^{11}C]AZ10419369 template dorsal brainstem VOI (see below).

3.3.6 Development of the 5-HT_{1B} PET template (Study II)

A [^{11}C]AZ10419369 template was created with T1-weighted MR images and parametric PET images of 52 subjects. T1-weighted MR images were normalized to the standard reference MNI-space[122] using FSL[130] (FSL 5.0, Oxford). After skull-stripping with BET[131], linear transformation was performed with FLIRT[132], followed by non-linear transformation with FNIRT[133]. The obtained non-linear transformation parameters were then used to normalize the co-registered parametric images into MNI-space. Subsequently, average images were created from both modalities.

3.3.7 Definition of brainstem VOIs (Study II)

Three VOIs were selected based on 2D ARG data reported in the literature[112,116,134] and visual inspection of the 3D [^{3}H]AZ10419369 ARG model: 1) a dorsal brainstem VOI, including dorsal and median raphe nuclei, periaqueductal gray, superior and inferior colliculi; 2) a substantia nigra VOI; and 3) a caudal brainstem VOI encompassing the 5-HT_{1B} receptors in the caudal part of the pons and medulla oblongata.

Estimated localization of VOIs was guided by landmarks reported in literature[18,135]. The final VOIs were generated and applied on test-retest data of 8 subjects by two previously reported

methods based on: 1) individual PET data[136] and 2) template PET data[137] of [^{11}C]AZ10419369 binding, as shown in Figure 9. Both methods were compared to results using the conventional method, i.e. a manually drawn VOI encompassing the dorsal and median raphe nuclei[104].

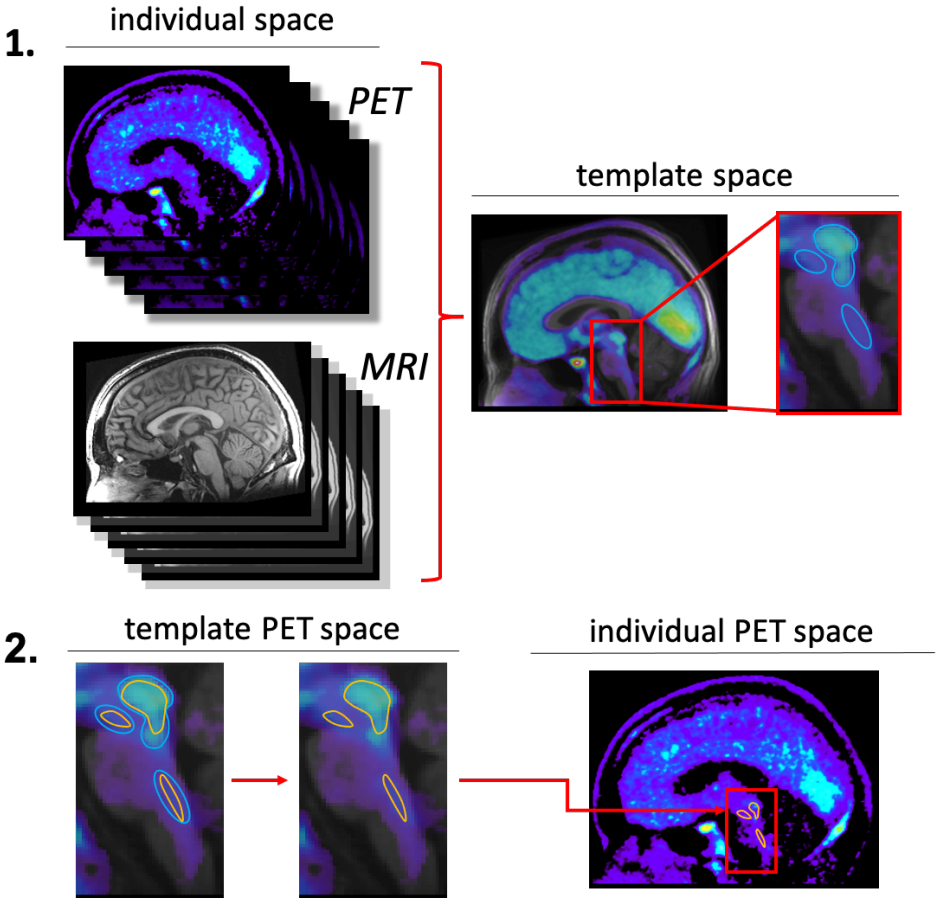

Figure 9: Template-based method. 1: PET images were co-registered to MRI data, averaged and normalized to MNI-space. Oversized VOIs were drawn on BP_{ND} maps. 2: VOIs were eroded based on volumes from literature findings[138–141] and highest radioligand binding. VOIs were then transformed to individual data. For the individual-based method, volumes were directly drawn and eroded on individual data.

3.4 FLOW CYTOMETRY (STUDY IV)

Flow Cytometry allows quantification of proteins expressed by individual cell populations, even in the case of intracellular proteins (as is the case for p11). The sample is mixed with antibodies conjugated to fluorescent dyes (fluorophores) and is directed to flow in a fluid stream through a beam of light. Emission spectra of the fluorophores are detected by the flow cytometer, which is calibrated to enable translation into a quantitative outcome measures (here: median fluorescence intensities (MFI)). The MFI provides a quantitative outcome measure for antigen expression per cell[142].

3.4.1 Subjects

Study IV was a secondary study of study III. All subjects in this study participated in study III and underwent examinations as described above. One subject from the ketamine group was excluded from the current study, as the MFIs of p11 at baseline were considered as outliers in all cell populations, resulting in 29 study participants.

3.4.2 PBMC Preparation

At baseline, within the same day as assessment of MADRS scores, venous blood samples were collected into tubes containing ethylenediaminetetraacetic acid. Using a standard procedure, samples were processed within 2 hours of collection. PBMCs were extracted by low-density gradient centrifugation using Lymphoprep (Axis-Shield). Isolated PBMCs were stored at −80°C in 90% fetal bovine serum/10% dimethyl sulfoxide until assay.

3.4.3 Sample preparation

PBMCs were processed as follows: frozen PBMC aliquots were thawed quickly and subsequently washed with PBS. Near-IR dead cell marker (Invitrogen, #L10119) was used to perform viability staining. After washing, cells were fixed and permeabilized with Cytofix/Cytoperm solution (BD, #554714) for 20 min, after which they were stained with monoclonal mouse anti-annexin II light chain (i.e. p11) antibody (5 µg/mL, clone 148; BD Transduction Laboratories™, #610071) or isotype control mouse IgG1 antibody (5 µg/mL, clone MOPC-21; BioLegend, #400124) for 45min at RT. Secondary staining was performed with APC-conjugated goat anti-mouse antibody (2 µg/mL; BioLegend, # 405308) for 30 min at RT. After washing and incubation in blocking buffer (1% mouse serum and 1% FBS in PBS), cells were stained with surface marker antibodies according to Table 4. After final washing, stained cells were analyzed using the multicolor flow cytometer Gallios (Beckman Coulter).

Table 4: Fluorophore conjugated antibodies and panel specifications

Channels			Panel 1			Panel 2		
No.	Laser (nm)	Filter (nm)	Antibody	Fluorophore	Clone	Antibody	Fluorophore	Clone
1	488	525/40	CD4	FITC	OKT4	CD56	FITC	B159
2	488	695/30	CD3	PerCP Cy5.5	UCHT1	CD16	PerCP	3G8
3	638	660/20	p11	APC		p11	APC	
4	638	755/LP	CD14	APC Cy7	MφP9	CD3	APC Cy7	UCHT1
5	405	550/40	CD8	BV510	SK1	CD14	BV510	M5E2

3.4.4 Panel optimization

Used lasers for excitation of fluorophores and filters for detection of fluorophore emission are displayed in Table 4. To minimize spectral overlap, the analysis was separated into one panel for T cells and one panel for NK-cells and monocytes. In channel 4, the dump channel, also viability stain was detected. Considerations for choosing optimal antibody-fluorophore combinations were separability by lasers/filters and pairing highly expressed antigens with dimmer fluorochromes (and vice versa). Moreover, the antibody for the protein of interest (p11) was conjugated towards a relatively bright fluorophore (APC). Antibody concentrations were titrated and separation of positive and negative cell populations was tested for by determining the separation index (SI)[143]:

$$SI = \frac{median_{pos} - median_{neg}}{\frac{84\%_{neg} - median_{neg}}{0.995}} \qquad 3.1$$

where $median_{pos}$ represents the median of the signal from the positive cell population, $median_{neg}$ the median of the signal from the negative cell population. The denominator represents the right hand of the distribution of the negative cell population. The higher the SI, the better the separation between positive and negative cell populations.

Even though fluorophores were chosen based on optimal separability by lasers and filters from each channel, emitted light by fluorophores from one channel can spill over into filters from another channel (Figure 10). This contribution of spill-out of each staining was determined by measuring the signal resulting of each stain separately, measured in the same sample. All the staining data used in the experiment was gathered to create a compensation matrix using FlowJo 10.4.2 (Tree Star Inc, Ashland), thereby semi-automatically correcting for spill-over.

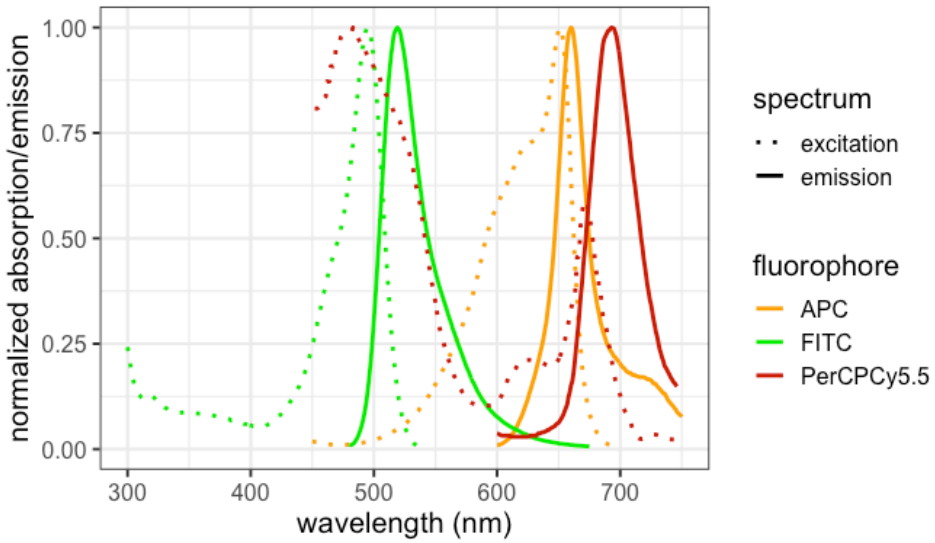

Figure 10: Excitation (dotted lines) and emission (solid lines) spectra from three fluorophores used in the flow cytometry experiment: FITC (green), APC (orange) and PerCP Cy5.5 (red). Note that although emission spectra from APC and PerCP Cy5.5 show a large overlap, their emission spectra differ. By excitation of these fluorophores at different laser wavelengths (Table 4), spill-in of signal is reduced. Fluorophore excitation and emission data downloaded from fluorophores.org

3.4.5 Flow Cytometry gating strategy

P11 levels were determined within each cell population using the following gating strategies: Cell populations are first gated to select single cells by excluding cells with increased forward scatter area vs height. Secondly, live cells gated as viability stain negative population. Then gating occurs based on size (forward scatter, FSC) and granularity (side scatter, SSC), in which lymphocytes have low FSC and SSC, while monocytes have higher SSC and high FSC. Furthermore, T-helper cells are gated as $CD14^{-}CD3^{+}CD4^{+}CD8^{-}$ lymphocytes, cytotoxic T cells as $CD14^{-}CD3^{+}CD4^{-}CD8^{+}$ lymphocytes, NK cells as $CD3^{-}CD14^{-}CD16^{+}CD56^{+}$ lymphocytes and monocytes as $CD3^{-}CD14^{+}CD56^{-}$ populations. The latter is further separated into classically activated ($CD14^{+}CD16^{-}$) and non-classically activated ($CD14^{+}CD16^{+}$) monocytes. P11 is detected using APC as secondary antigen.

Controls used for gating were the isotype control and *fluorescence minus one*-controls[144]: samples containing all antibody conjugates except the one which is of interest in the channel. Analyses were performed in FlowJo 10.4.2. Total p11 levels were calculated by multiplying the percentage of p11+ cells by the median fluorescence intensity of antibody staining. Antibody specificity towards p11 was confirmed and MFI of p11 was determined in specific peaks (peaks not overlapping with the isotype control).

3.5 STATISTICAL ANALYSIS

Statistical analysis was performed using R (R Development Core Team, 2020). For all statistical tests, the α-level was set to 0.05.

3.5.1 Comparison of four subject groups (study I)

To compare specific binding between the four subject groups (bipolar disorder, MDD, schizophrenia and healthy control), ANOVA tests were carried out together with a Tukey Post-Hoc test to examine all pair wise comparisons and to correct for multiple comparisons.

A paired Student's t-test was performed to calculate differences between specific binding in cortical layers and Cohen's D was calculated to determine the effect size.

Mann-Whitney tests were used to calculate differences for comparisons of genders, where data showed non-normal distribution. For this data Cliff's δ was calculated to determine the effect size. When analyzing differences between subject groups, p-values were adjusted for multiple comparisons using Bonferroni's method.

3.5.2 Test-retest metrics (study II)

In study II, the following metrics were defined:

- Coefficient of Variation (COV): shows variation between subjects and is calculated by dividing the SD by the mean BP_{ND}.
- Average Absolute Percentage Difference (APD): represents an absolute value of normalized intra-subject differences.

- Intraclass Correlation Coefficient (ICC): a measure of the inter-subject differentiability. In this case the one-way random effects model with single measures is used (i.e. ICC(1,1)). ICC values range from 0-1, with 1 indicating perfect inter-subject differentiability.
- Standard Error of Measurement (SEM): an estimate of precision of individual outcome values and is given in the unit of the measurement (here: BP_{ND}).
- Minimal Detectable difference (MD): difference between two measurements necessary to be considered greater than random measurement error, according to a 95% confidence interval[145]. The MD is here given as percentage of the average BP_{ND}.

3.5.3 Comparison between change scores in two study groups (study III-IV)

In study III, differences in regional BP_{ND}s, when corrected for the effect in the placebo group, were tested for significance by calculating the group (ketamine vs placebo) x time (pre vs post intervention) interaction effect in a repeated measures ANOVA (RM ANOVA).

In study IV, non-parametric approaches were used as the requirement of normal distribution of MFI data was not met in all cell populations. Differences in change scores of MFI between the ketamine and placebo group were tested for using the two-sided Mann-Whitney U test. Additionally, differences in change scores between both treatment groups were also tested for using a linear mixed model. In this model, p11 level post-treatment was used as outcome measure; explained by group (ketamine vs placebo), p11 level pre-treatment and cell type as fixed effects; a group by cell type interaction to test the effect of treatment in each separate cell type and subject included as random effect (varying intercept). To reduce skewness in the data and stabilize variance across different cell types, the natural log of p11 values was used in the linear mixed model analysis.

For exploratory analysis, differences in regional BP_{ND} (study III) and MFI (study IV) within the treatment group were tested using two-tailed paired Student's t-tests and two-sided Wilcoxon Signed Rank Test, respectively.

3.5.4 Correlations

Pearson's correlation coefficient was calculated to test for correlation of age with specific binding (study I) or BP_{ND} (study II).

Correlations between MADRS scores and regional BP_{ND}s (study III) or MFI values (study IV) were tested for significance using the Pearson correlation and Spearman's *rho* method, respectively.

4 RESULTS AND COMMENTS

4.1 STUDY I

5-HT$_{1B}$ receptor binding was visualized using high-resolution ARG and the radioligand [^{3}H]AZ10419369 in tissue of the ACC in subjects with bipolar disorder, MDD, schizophrenia and healthy controls. Next to this, ARG binding was quantified and a comparison was made between binding distribution between patient groups, in relation to age and gender.

A significantly higher specific binding of 5-HT$_{1B}$ receptor was found in the outer ACC layers compared to the inner ACC layers ($p_{adjusted} < 0.001$) (Figure 11), while no significant difference between patient groups was found in both cortical layers and total cortical binding. A gender difference was found, which was mostly profound in subjects diagnosed with MDD. As the tissue used in this study was distributed to several institutions, performing a wide variety of experiments, it was possible to perform an exploratory correlation analysis with other autoradiographic neuroreceptor binding distributions (8 studies available). A significant moderate correlation was found with glutamatergic NMDA receptor distribution ([^{3}H]MK801 binding), of which only binding in the outer cortical layers survived correction for multiple comparisons ($p_{adjusted} = 0.04$, $r = 0.41$).

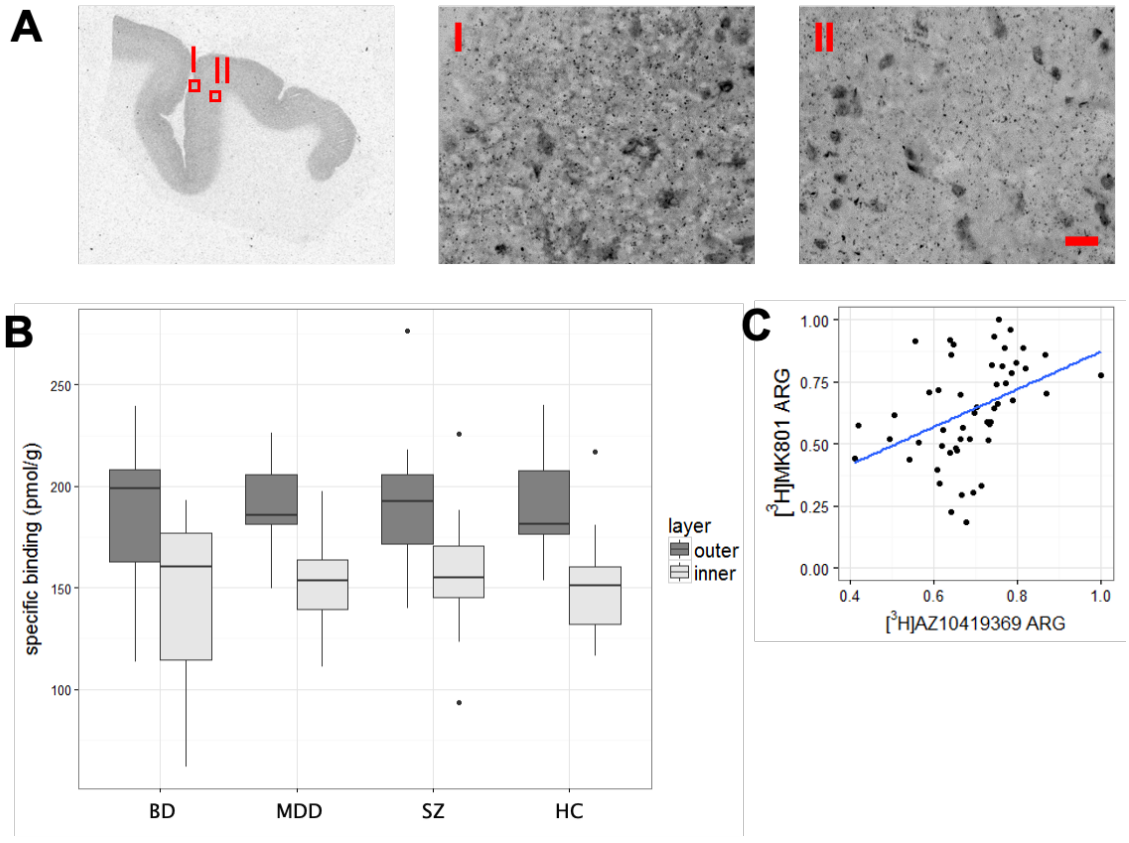

Figure 11: A) Representative tissue slice showing [3H]AZ10419369 ARG binding distribution. Middle and right: 35x magnification showing Nissl staining and high-resolution ARG (small dots) in outer (I) and inner layer (II) (scale bar = 20 µm).
B) [3H]AZ10419369 ARG binding distribution in tissue from subjects with bipolar disorder (BD), major depressive disorder (MDD), schizophrenia (SZ) and healthy controls (HC).
C) Plot with normalized specific binding values of [^{3}H]AZ10419369 vs [^{3}H]MK801 in outer layer.

No differentiation could be made in 5-HT_{1B} receptor binding between patient groups or compared to controls. However, a recent PET study from our group has shown 20% lower 5-HT_{1B} concentrations in the ACC in MDD subjects compared to healthy controls[43]. The discrepancy compared to the *in vivo* results were not considered to be a lack of power in this *in vitro* ARG study, nor was the variance between subjects higher in this study. Possible reasons for the divergent findings could be medication use and higher severity of depression in this study. The latter factor would imply alterations in 5-HT_{1B} being a state marker of depression, rather than a trait marker. Previously reported negative correlation between 5-HT_{1B} receptor binding and age in healthy controls[146] and MDD subjects[43], were also not found in this study. This could be caused by the differences in methods for ROI delineation in ARG and PET: when using PET, age-affected alterations in brain volumes can be adjusted for using a PVE correcting algorithm, whereas in ARG gray matter volume is directly delineated.

4.2 STUDY II

The aim of this study was to improve quantification of regional [^{11}C]AZ10419369 PET data in the brainstem. For this purpose, a 3D [^{3}H]AZ10419369 ARG model was used to guide brainstem VOI selection for [^{11}C]AZ10419369 PET image analysis, in which two different semi-automatic VOI-defining methods, based on individual[136] or on template[137] PET data, were tested and compared to a conventional method using manual delineation[104].

In vivo PET and *in vitro* ARG are affected by distinct factors, such as potential receptor degradation in *post mortem* tissue when using ARG and binding of endogenous compounds *in vivo* when using PET. Moreover, the different outcome values of both modalities are defined using different quantification methods, as discussed in the introduction. Therefore, an evaluation was performed on to what extent receptor distribution measured with ARG can be used to guide VOI definition in *in vivo* receptor quantification with PET. The relationship was tested between *post mortem* [^{3}H]AZ10419369 specific binding in whole hemisphere ARG data of three subjects and regional BP_{ND} [^{11}C]AZ10419369 of test-retest PET data. Binding was measured in nine VOIs outside the brainstem and showed a strong significant correlation ($r=0.78$, $p=0.013$).

With the 3D ARG model of [^{3}H]AZ10419369 binding, the distribution of the 5-HT_{1B} receptor in brainstem tissue was visualized at high spatial resolution. This model showed continuous distribution of [^{3}H]AZ10419369 binding in the dorsal midbrain and from the caudal area of the pons to the medulla oblongata (Figure 12A). Together with findings in literature, three appropriate VOIs were selected for quantification with PET: dorsal brainstem, substantia nigra and caudal brainstem (Figure 12B).

Delineation of the VOIs was performed on PET data using the two semi-automatic methods. For delineation of the dorsal brainstem VOI, both semi-automatic methods showed improvements in reliability metrics compared to the conventional method (Figure 13). Both semi-automatic methods provided BP_{ND} values that were consistently higher and presented a consistently lower COV than those obtained with the conventional method. This effect was strongest in the individual-based method for all VOIs. Reliability for quantification in the dorsal and caudal brainstem VOIs was high using both semi-automatic methods. However,

quantification in the substantia nigra VOI resulted in moderate reliability outcomes. Future studies should examine other possibilities to quantify this VOI with higher reliability.

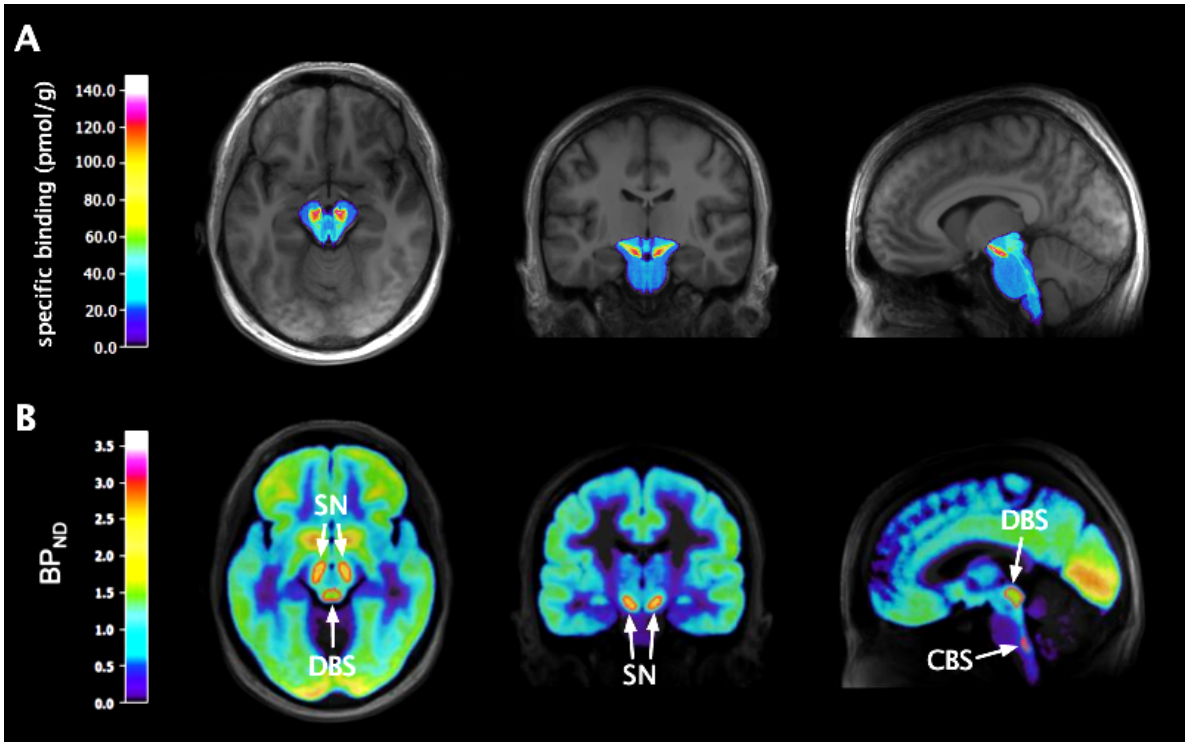

Figure 12: A) 3D model of [^{3}H]AZ10419369 ARG specific binding. B) Template [^{11}C]AZ10419369 PET data with in red the Volumes of Interest DBS (dorsal brainstem), CBS (caudal brainstem) and SN (substantia nigra). Both modalities are overlayed on template MRI data

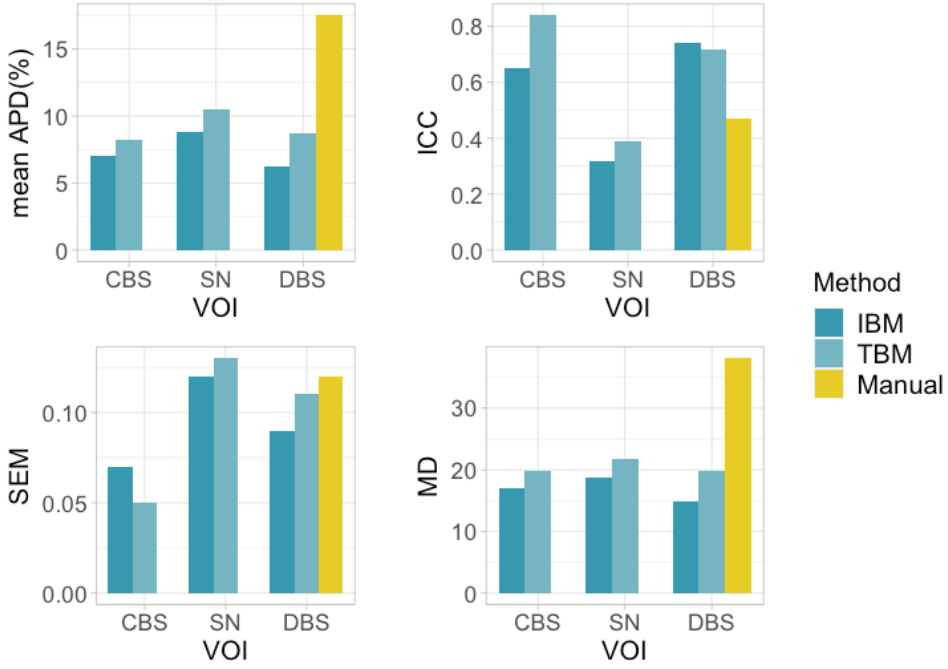

Figure 13: Bar plots showing reliability outcomes for each Volume of Interest (VOI) using the individual-based method (IBM), template-based method (TBM) and a manual method.
APD: Absolute Percentage Difference; CBS: caudal brainstem; DBS: dorsal brainstem; ICC: Intraclass Correlation Coefficient; SEM: Standard Error of Measurement; SN: substantia nigra; MD: Minimal Detectable difference

Although good reliability outcomes were seen for the individual-based method, an advantage of the template-based method is its easy implementation for future [^{11}C]AZ10419369 PET data. VOIs based on individual data have to be generated for every new subject and could therefore be more prone to user error.

A comparison of normalized PET template binding data in the eroded VOIs with normalized 3D ARG signal in MNI-space showed that, throughout the brainstem, normalized BP_{ND} values were relatively higher than normalized specific binding values, particularly in the dorsal and caudal brainstem VOIs (Figure 14). These areas could be most influenced by the resolution limitation of PET.

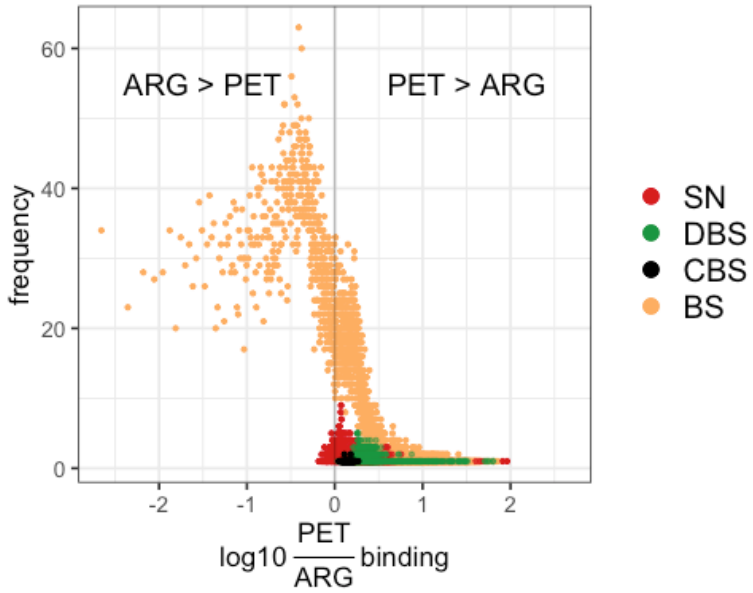

Figure 14: Frequency of outcomes for log10 ratio of [^{11}C]AZ10419369 PET BP_{ND} over [^{3}H]AZ10419369 3D ARG specific binding in each voxel within the different analyzed volumes of interest: substantia nigra (SN), dorsal brainstem (DBS), caudal brainstem (CBS) and rest of the brainstem (BS).

4.3 STUDY III

In this study, the effect of a subanaesthetic dose of ketamine on 5-HT_{1B} receptor binding using [^{11}C]AZ10419369 PET was examined in SSRI-treatment resistant patients with MDD, in relation to treatment response.

After the first intervention, subjects receiving ketamine showed a significant decrease in MADRS-scores ($p_{adjusted} < 0.001$; Figure 15). In the placebo group, 4 subjects believed they received active treatment, compared to 19 subjects in the ketamine group. MADRS-scores did not change significantly in the placebo group.

No significant difference in BP_{ND} change over time between the ketamine and the placebo group was found in the pre-selected VOIs. Exploratory analysis within treatment groups showed a BP_{ND} increase of 16.7% in the hippocampus after ketamine treatment (Figure 16). This may reflect increased 5-HT_{1B} receptor densities (or increased affinity of the radioligand

towards the receptor) or reduced serotonin concentration available to displace [^{11}C]AZ10419369 binding. Therefore, this result differs from previous findings in non-human primates, where ketamine infusion led to increased 5-HT$_{1B}$ receptor binding in the ventral striatum (VST)[76]. It should be noted that there are various important difference between both studies: in the current study subanesthetic doses of ketamine were used instead of anesthetic doses and [^{11}C]AZ10419369 binding was studied after 1-2 days instead of during ketamine infusion.

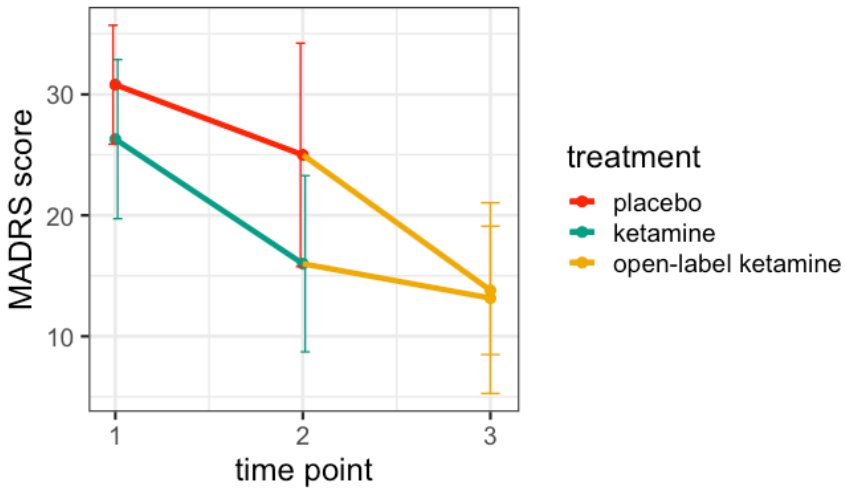

Figure 15: Montgomery-Åsberg Depression Rating Scale (MADRS) scores after treatment with placebo or ketamine, followed by open-label ketamine treatment. Error bars showing SD.

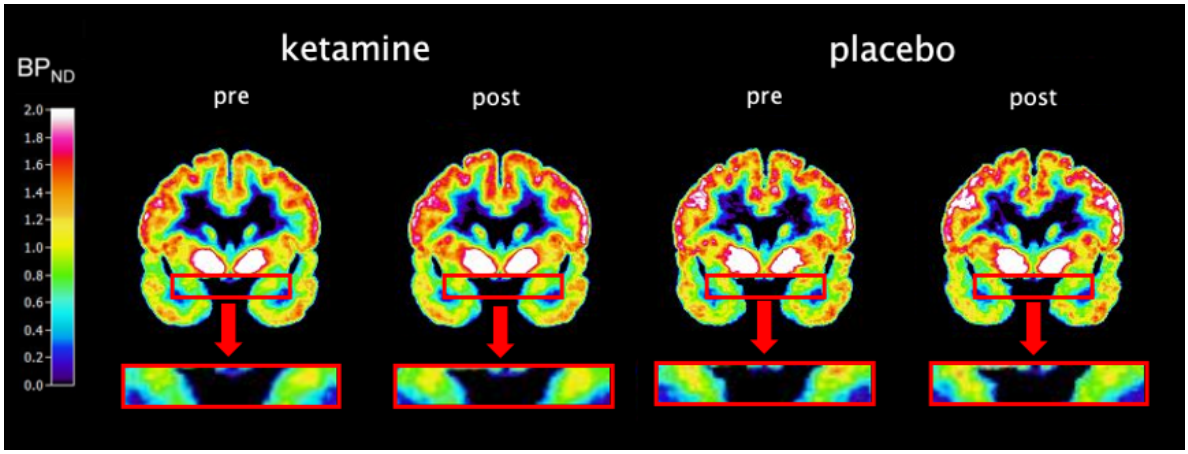

Figure 16: [^{11}C]AZ10419369 binding in the ketamine and placebo group, before and after treatment.

Baseline 5-HT$_{1B}$ receptor binding correlated significantly with baseline MDD symptom ratings (ρ=-0.426, p=0.019) and with reduction of MDD symptom ratings after ketamine treatment ketamine (ρ=-0.644, p=0.002). The latter correlation shows therefore an association between low baseline 5-HT$_{1B}$ receptor binding values and stronger improvements in MDD symptoms. The correlation of low baseline 5-HT$_{1B}$ receptor binding with high MADRS-scores, thus more severe MDD symptoms, seems in line with previous findings from Murrough et al. (2011)[44], who showed significantly lower 5-HT$_{1B}$ receptor binding in MDD subjects compared to healthy controls, although no correlation with clinical measures was found.

Baseline MADRS was significantly different in both study groups. Since baseline [^{11}C]AZ10419369 was shown to be correlated with baseline or changes in MADRS scores, this could have influenced results. However, when factoring in baseline MADRS scores in the analysis of BP_{ND} changes in both study groups, this did not change the results. The relatively high variance of MADRS changes in both treatment groups could have likely influenced the results, especially for the placebo group, although a placebo effect on BP_{ND} values was not seen.

4.4 STUDY IV

Study IV was a secondary study of study III. The aim of the study was to examine the effect of ketamine on peripheral p11 levels in separate white blood cell populations, in relation to treatment response. This enabled the examination of the possibility that peripheral p11 could serve as a biomarker of antidepressant response of ketamine in MDD patients. P11 levels were determined using multicolor Flow Cytometry.

In none of the studied cell populations, a significant difference in p11 level changes was seen between the ketamine and placebo group. Within treatment groups, median p11 levels were decreased after ketamine treatment in $CD8^+$ cells (cytotoxic T cells; p=0.045) and $CD4^+$ cells (T-helper cells; p=0.002) (Figure 17). When comparing p11 levels with treatment response, a significant correlation was found between baseline p11 levels in cytotoxic T cells and changes in MADRS scores after ketamine treatment (rho=-0.601, p=0.007). Higher baseline p11 levels were associated with a greater improvement in MDD symptoms. Removal of the outlier decreased the difference in baseline MADRS scores between both study groups, as seen in study III, resulting in a non-significant difference in baseline MADRS.

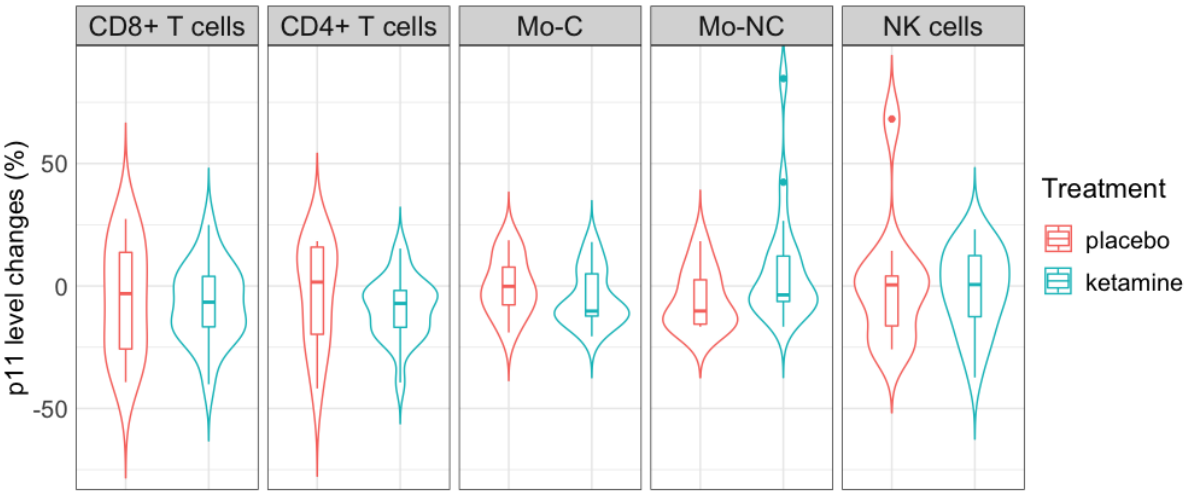

Figure 17*:* Violin plots showing the distribution of p11 level changes after treatment with ketamine and placebo in cytotoxic T cells ($CD8^+$), T-helper cells ($CD4^+$), Classically activated monocytes (Mo-C), Non-classically activated monocytes (Mo-NC) and Natural Killer cells (NK). Boxes within the violin plot represent the interquartile range, with horizontal line representing the median and vertical lines representing the values within 1.5 times of the interquartile range. Outliers are shown as single dots.

Although not significantly different from changes seen in the placebo group, the decrease in p11 levels after treatment is in line with what was found in a study on the effect of the SSRI citalopram on p11 levels[59], although no correlations were found between baseline p11 levels and MADRS levels or changes in the citalopram study. In the current study, a reduction of p11 levels was found in T cells of patients in the ketamine treatment group, whereas citalopram was reported to mainly regulate p11 in NK cells and monocytes[59]. This implies a different role of p11 in both drugs and emphasizes cell-type regulations of p11 by therapies with distinct mechanisms of action. Further studies, controlled by a placebo group, should clarify these findings.

5 CONCLUSIONS AND POINTS OF PERSPECTIVES

In this thesis, *in vivo* and *in vitro* techniques were used to study levels of the 5-HT_{1B} receptor and the related protein p11 in relation to MDD and treatment with ketamine. In study I, the differentiability of 5-HT_{1B} in MDD subjects compared to other psychiatric disorders and healthy subjects was studied using ARG. In study II, an improved method was proposed for quantification of 5-HT_{1B} receptor densities in the brainstem using PET. In study III and IV, a potential role of cerebral 5-HT_{1B} receptor binding and p11 levels in the antidepressant mechanism of action and treatment response of ketamine were studied.

Study I: A distribution pattern of 5-HT_{1B} receptor binding was shown in the ACC, with significantly higher 5-HT_{1B} receptor binding in supragranular layers compared to infragranular layers. Comparison of this distribution pattern with available ARG data on the same tissue and in similar ROIs showed a significant correlation with the binding pattern of the NMDA receptor. Therefore, it is of interest to further investigate the role of 5-HT_{1B} receptors on glutamate transmission in the ACC.

5-HT_{1B} receptor binding distributions and densities in total ACC gray matter did not significantly differ between subjects with bipolar disorder, schizophrenia, MDD and healthy controls. This finding differs from a previous PET study showing significantly lower 5-HT_{1B} receptor binding in unmedicated MDD subjects compared to healthy subjects[43]. Therefore, it would be of interest to study the differences between these studies, such as the effect of chronic medication use on 5-HT_{1B} receptor binding.

In female subjects, significantly lower 5-HT_{1B} receptor binding was found than in male subjects. Post-hoc analysis in the different treatment groups showed that this finding was driven by the MDD group. No differences in 5-HT_{1B} binding between sexes in MDD subjects has been previously reported, therefore it would be of interest to investigate this further in future studies.

Study II: Based on a 3D [^{3}H]AZ10419369 ARG model from *post mortem* brainstem tissue and literature findings, three appropriate VOIs for [^{11}C]AZ10419369 PET quantification were selected: a dorsal brainstem VOI, the substantia nigra and a caudal brainstem VOI. Two previously reported semi-automatic quantification methods, based on individual PET data[136] and based on template data[137], used for quantification of 5-HTT binding data were tested. Comparison with a conventional manual method[104] showed improved reliability for both semi-automatic methods. Reliability outcomes were particularly high for the dorsal and caudal brainstem VOIs. Reliability of quantification in the substantia nigra VOI was moderate and should be improved using alternative methods. Although the method based on individual PET data showed in general highest reliability outcomes, the template-based PET method provides easy implementation and is less prone to user-error.

Template VOIs based on [^{11}C]AZ10419369 PET data of 52 healthy subjects are available for use in future PET studies. This study used data of healthy subjects for both creation of the template and testing the methods. Therefore, future studies should confirm the reliability in subjects with psychiatric or neurological disorders.

Study III: In this randomized placebo-controlled PET study, the effect of ketamine on [^{11}C]AZ10419369 binding was studied in patients with SSRI-resistant MDD. 5-HT_{1B} receptor binding did not significantly change in the subjects treated with ketamine compared to placebo. Exploratory analysis within the ketamine group showed an increase in 5-HT_{1B} binding in the hippocampus after treatment. Further studies should clarify if the discrepancy with a study in non-human primates[76] is a result of different dosages of ketamine or different timing of the PET examination after ketamine administration.

Baseline 5-HT_{1B} binding in VST correlated inversely with baseline MDD symptoms and reduction of depressive symptoms after ketamine treatment. Future studies should be conducted on the role of 5-HT_{1B} receptors in the antidepressant mechanism of action of ketamine and should clarify if 5-HT_{1B} receptor binding could be used to predict ketamine treatment response for SSRI-resistant MDD subjects.

Study IV: Peripheral p11 levels were measured in the subjects from study III, before and after treatment with ketamine or placebo. P11 levels did not significantly change in MDD subjects treated with ketamine when compared to placebo. When only testing for within group changes, median p11 levels were shown to be decreased after ketamine treatment in both cytotoxic T cell and T-helper cell populations. A previous study showed a decrease of peripheral p11 levels in NK cells and monocytes after treatment with the SSRI citalopram[59]. Future studies should clarify if p11 could have a cell-type differentiable role in the antidepressant action of these and other antidepressant treatment options.

Baseline p11 levels in cytotoxic T cells correlated significantly with changes in depressive symptoms, with higher baseline p11 levels being associated with greater improvements in MDD symptoms. This finding should be replicated in future studies to investigate if peripheral p11 levels in cytotoxic T cells could be used to predict treatment outcomes for ketamine treatment in SSRI-resistant MDD subjects.

6 ACKNOWLEDGEMENTS

This work is the result of efforts from so many people and I'm forever grateful for all their contributions to my PhD. It has been an honour to work with and learn from many inspiring people during the journey of this PhD work.

First of all, I would like to thank my main supervisor, *Johan Lundberg*. You have been an amazing and inspiring supervisor for me these past years. Thank you for believing in me back when I started just fresh from university and all those times when research took unexpected ways. You have giving me the freedom to learn and explore, while providing guidance where I needed it. Whenever I would get stuck with a project, you were always (really always!) available for a good discussion, support and a good dose of positivity to help make things work.

My co-supervisor, *Marie Svedberg*, thank you for warmly welcoming me to the research group when I was still a naïve young Master student. You've introduced me to this research field with great enthusiasm and triggered me to go into research with your interesting projects. I am so grateful that you wanted to (co-)supervise me again.

Thank you to my other co-supervisor, *Andrea Varrone*, I have learned so much from your great expertise in PET (and now also in 3D ARG?). Thank you for your valuable input, patience, creative ideas and guidance that helped me go through a project that seemed impossible at times. You're dedication is really inspirational and motivate your students to do better research.

Per Svenningsson, my third co-supervisor, thank you for introducing me to your lab, the good scientific discussions, your interest and for always making time despite your busy schedule. I have learned a great deal from your expertise and I am very thankful for the interesting projects I could do at your lab, which added an extra dimension to what I learned during my PhD.

I'm very grateful for *Siv Eriksson* and *Åsa Södergren* for helping to teach me ARG, all your help and good talks during the ARG experiments and the many hours at the cryostat. Thank you also for your patience with my poor Swedish and letting me take over your lab at times by occupying all the benches with incubating brain slices. Thank you *Patricia Miranda-Azpiazu* for your great spirit and company in the lab. *Katarina Varnäs*, with your expertise in both ARG & PET your help was invaluable for my research. Thank you *Holly Green, Dejan Mamula* and *Haitang Jiang* for your inspiring dedication, good company and long hours in your lab.

The radiochemists, thank you for your hard work as foundation for the ARG and PET experiments, but also for the great company and football trainings during my Master's project: *Guennadi Jogolev, Vladimir Stepanov, Arsalan Amir, Magnus Schou, Peter Johnström, Zhisheng Jia, Sangram Nag, Mahabuba Jahan, Johan Ulin, Mélodie Ferrat, Youssef el Khoury, Prodip Datta* and *Mikhael Kondrashov*.

Thank you to all the research nurses for all your valuable work for the PET examinations and being such nice people: *Nina Knave, Malena Kjellén, Opokua Britton-Cavaco and Karin Olsson*. *Karin Zahir* and *Hillevi Andersson-Sand*, thank you for all the help with the too many forms and so many other practical things. *Urban Hansson,* thank you for saving my computer again and again. *Göran Rosenqvist*, thank you for the many many PET data reconstructions.

Zsolt Cselényi, thank you for your amazing work on the PET analysis pipelines and your interest and help in my research.

A big thank you to my roommates (and those pretending to be) from room 1300.5: *Ämma Tangen, Max Andersson, Jonas Svensson, Pontus-Plavén Sigray, Granville Matheson, Patrik Fazio and Vera Kerstens*. For those who joined the gang later, *Maria Lee, Tove Freiburghaus, Gina Griffioen, Joachim Brumberg* and *Martin Gärde*, thank you for keeping the 1300.5 spirit going strong. Thank you for all the nice lunch conversations and fun times after work. You guys have made it so much more fun to work, even at times when doing research was a struggle. Thank you also for your passion and dedication to discuss research, sharing life-saving scripts and help each other not getting lost in the garden of forking paths. I even want to thank you for those times keeping me from my work, with such endless but very important discussions about the habenula, Bayesian magic, best coffee (machine) brands, the private lives of MOOC teachers and let's also not forget the musical delights with which we created awesome dissertation party songs. Thank you to the lunch running gang for help refreshing the mind and promising time and time again that the hill will go downwards from now on.

The former 0th floor lunch gang and good researchers: *Anton Forsberg-Morén, Miklós Tóth*, *Lenke Tari, Kai-Chun Yang*, *Mikael Tiger*, *Karin Collste, Pauliina Victorsson, Zsolt Sarnyai* and *Jenny Häggkvist,* thank you for your warm company and good discussions.

Thank you *Christer Halldin* and *Lars Farde,* for your leadership and inspiring the PET-group with good research. Thank you to other (former) members of the PET-group for your interest, your contribution to my research work or from your work from which I learned a lot: *Simon Cervenka, Balazs Gulyas, Jacqueline Borg, Per Stenkrona, Aurelija Jučaite*, *Magdalena Nord, Patrik Mattson, Bogdan Mitran, Carl-Johan Ekman, Hampus Yngwe, Carsten Steiger, Ryosuke Arakawa, Sjoerd Finnema, Akahiro Takano* and *Martin Schain*.

I would also like to show my gratitude to all the people who have volunteered to give their time, effort, blood or brain tissue to research. Without these people this PhD would not have been possible!

Thank you to my friends in Stockholm, for making this Swedish journey fun since the very first day: the former Vårbergers *Eleni, Vasilis, Aliki, Sunjay, Max;* my friends since the first PhD day and former roomy *Hannes* and *Irem*; my Austrian family *Benny, Fee, Olivia and Maya;* the former and current Dutch borrel-mates & friends *Juliëtte, Boudewijn, Tosca, Jon, Florentine, Claudia, Maarten, Brechtje, Jenny, Stefan & Bas;* and the fabulous Fredhäll gang *Fifi, Joanna & Kristin* and their families.

Thank you to my friends in the Netherlands, for being such amazing people and the nice times we spent in Stockholm and back home: especially the *Gioia* ladies, *bestuurtje 129* and *Mies*.

Last but not least I would like to thank my lovely family. My family back home, for being there for me even when being far away. My love Thomas, my crazy sambo, thank you for joining me in this Swedish adventure and always being there for me. This thesis would not have existed without your support and endless positivity. Thank you Filippa, for being the best that has ever happened to me.

7 REFERENCES

1. WHO. *Depression and Other Common Mental Disorders: Global Health Estimates. Geneva: World Health Organization*. 2017.
2. Papakostas GI, Ionescu DF. Towards new mechanisms: An update on therapeutics for treatment-resistant major depressive disorder. *Mol Psychiatry*. 2015;20:1142–1150.
3. Al-Harbi KS. Treatment-resistant depression: Therapeutic trends, challenges, and future directions. *Patient Prefer Adherence*. 2012;6:369-388.
4. Rush AJ, Trivedi MH, Wisniewski SR, et al. Acute and longer-term outcomes in depressed outpatients requiring one or several treatment steps: A STAR*D report. *Am J Psychiatry*. 2006;163(11):1905-1917.
5. Dimasi JA, Feldman L, Seckler A, Wilson A. Trends in risks associated with new drug development: Success rates for investigational drugs. *Clin Pharmacol Ther*. 2010;87(3):272-277.
6. Krystal JH, Abdallah CG, Sanacora G, Charney DS, Duman RS. Ketamine: A Paradigm Shift for Depression Research and Treatment. *Neuron*. 2019;101:774-778.
7. Berman RM, Cappiello A, Anand A, et al. Antidepressant effects of ketamine in depressed patients. *Soc Biol Psychiatry*. 2000;47(4):351-354.
8. Caddy C, Amit BH, McCloud TL, et al. Ketamine and other glutamate receptor modulators for depression in adults. *Cochrane database Syst Rev*. 2015;9:CD011612.
9. *Diagnostic and Statistical Manual of Mental Disorders, 5th Edition: DSM-5*. American Psychiatric Association; 2013.
10. Otte C, Gold SM, Penninx BW, et al. Major depressive disorder. *Nat Rev Dis Prim*. 2016; 2:16065.
11. Belmaker RH, Agam G. Major depressive disorder. *N Engl J Med*. 2008; 358(1):55-68.
12. Gill K, Bennett-Penn L, Bernstein CA. Gabbard's Treatments of Psychiatric Disorders, DSM-5 Edition. *J Clin Psychiatry*. 2015;76(10):e1325-e1326.
13. Schildkraut JJ. The Catecholamine Hypothesis of Affective Disorders: A Review Of Supporting Evidence. *Am J Psychiatry*. 1965;122:509-522.
14. Coppen A. The biochemistry of affective disorders. *Br J Psychiatry*. 1967; 113(504):1237-64.
15. Lapin IP, Oxenkrug GF. Intensification of the Central Serotoninergic Processes as a Possible Determinant of the thymoleptic effect. *Lancet*. 1969;293(7586):132-136.
16. Delgado PL, Price LH, Miller HL, et al. Serotonin and the Neurobiology of Depression: Effects of Tryptophan Depletion in Drug-Free Depressed Patients. *Arch Gen Psychiatry*. 1994; 51(11):865-74.
17. Berger M, Gray JA, Roth BL. The expanded biology of serotonin. *Annu Rev Med*. 2009;60(August 2016):355-366.
18. Törk I. Anatomy of the Serotonergic System. *Ann N Y Acad Sci*. 1990;600(1):9-34.
19. Alexander SPH, Davenport AP, Kelly E, et al. The Concise Guide to Pharmacology 2015/16: G protein-coupled receptors. *Br J Pharmacol*. 2015;172(24):5759-5763.
20. Kambeitz JP, Howes OD. The serotonin transporter in depression: Meta-analysis of in vivo and post mortem findings and implications for understanding and treating depression. *J Affect Disord*. 2015; 186:358-66
21. Wang L, Zhou C, Zhu D, et al. Serotonin-1A receptor alterations in depression: A meta-analysis of molecular imaging studies. *BMC Psychiatry*. 2016; 16(1):319

22. Savitz JB, Drevets WC. Neuroreceptor imaging in depression. *Neurobiol Dis*. 2013;52:49-65.
23. Murrough JW, Neumeister A. The serotonin 1B receptor: A new target for depression therapeutics? *Biol Psychiatry*. 2011;69(8):714-715
24. Tiger M, Varnäs K, Okubo Y, Lundberg J. The 5-HT(1B) receptor - a potential target for antidepressant treatment. *Psychopharmacology (Berl)*. 2018;235(5):1317-1334.
25. Sari Y. Serotonin1B receptors: from protein to physiological function and behavior. *Neurosci Biobehav Rev*. 2004;28(6):565-582.
26. Boschert U, Amara D a, Segu L, Hen R. The mouse 5-hydroxytryptamine1B receptor is localized predominantly on axon terminals. *Neuroscience*. 1994;58(1):167-182
27. Varnäs K, Hurd YL, Hall H. Regional expression of 5-HT1B receptor mRNA in the human brain. *Synapse*. 2005;56(1):21-28.
28. Varnäs K, Nyberg S, Halldin C, et al. Quantitative analysis of [11C]AZ10419369 binding to 5-HT1B receptors in human brain. *J Cereb Blood Flow Metab*. 2011;31(1):113-123.
29. Saudou F, Amara DA, Dierich A, et al. Enhanced aggressive behavior in mice lacking 5-HT1B receptor. *Science*. 1994;265(5180):1875-1878. doi:10.1126/science.8091214
30. Hoplight BJ, Vincow ES, Neumaier JF. The effects of SB 224289 on anxiety and cocaine-related behaviors in a novel object task. *Physiol Behav*. 2005;84(5):707-714.
31. Da Cunha-Bang S, Hjordt LV, Perfalk E, et al. Serotonin 1B Receptor Binding Is Associated With Trait Anger and Level of Psychopathy in Violent Offenders. *Biological Psychiatry*. 2016;82(4):267-274.
32. Varrone A, Svenningsson P, Marklund P, et al. 5-HT1B receptor imaging and cognition: a positron emission tomography study in control subjects and Parkinson's disease patients. *Synapse*. 2015; 69(7):365-74
33. Malleret G, Hen R, Guillou JL, Segu L, Buhot MC. 5-HT1B receptor knock-out mice exhibit increased exploratory activity and enhanced spatial memory performance in the Morris water maze. *J Neurosci*. 1999;19(14):6157-6168.
34. Edwards E, Harkins K, Wright G, Henn FA. 5-HT1b, receptors in an animal model of depression. *Neuropharmacology*. 1991;30(1):101-105.
35. Nishi K, Kanemaru K, Diksic M. A genetic rat model of depression, Flinders sensitive line, has a lower density of 5-HT1A receptors, but a higher density of 5-HT1B receptors, compared to control rats. *Neurochem Int*. 2009;54(5-6):299-307.
36. Shrestha SS, Pine DS, Luckenbaugh DA, et al. Antidepressant effects on serotonin 1A/1B receptors in the rat brain using a gene x environment model. *Neurosci Lett*. 2014;559:163-168.
37. Neumaier JF, Petty F, Kramer GL, Szot P, Hamblin MW. Learned helplessness increases 5-hydroxytryptamine1B receptor mRNA levels in the rat dorsal raphe nucleus. *Biol Psychiatry*. 1997;51(11):902-908.
38. Neumaier JF, Edwards E, Plotsky PM. 5-HT1B mRNA regulation in two animal models of altered stress reactivity. *Biol Psychiatry*. 2002;51(11):902-908.
39. McDevitt RA, Hiroi R, MacKenzie SM, et al. Serotonin 1B autoreceptors originating in the caudal dorsal raphe nucleus reduce expression of fear and depression-like behavior. *Biol Psychiatry*. 2011;69(8):780-787.
40. Huang Y, Oquendo M a, Friedman JMH, et al. Substance abuse disorder and major depression are associated with the human 5-HT1B receptor gene (HTR1B) G861C

polymorphism. *Neuropsychopharmacology*. 2003;28(1):163-169.
41. Anisman H, Du L, Palkovits M, et al. Serotonin receptor subtype and p11 mRNA expression in stress-relevant brain regions of suicide and control subjects. *J Psychiatry Neurosci*. 2008;33(2):131-141.
42. Lopez-Figueroa AL, Norton CS, Lopez-Figueroa MO, et al. Serotonin 5-HT1A, 5-HT1B, and 5-HT2A receptor mRNA expression in subjects with major depression, bipolar disorder, and schizophrenia. *Biol Psychiatry*. 2004;55(3):225-233.
43. Tiger M, Rück C, Varrone A, et al. Lower serotonin1B receptor binding potential in the anterior cingulate cortex in major depressive disorder. *Psychiatry Res Neuroimaging*. 2016;253:36-42.
44. Murrough JW, Henry S, Hu J, et al. Reduced ventral striatal/ventral pallidal serotonin1B receptor binding potential in major depressive disorder. *Psychopharmacology (Berl)*. 2011;213(2-3):547-553.
45. Tiger M, Rück C, Forsberg A, et al. Reduced 5-HT(1B) receptor binding in the dorsal brain stem after cognitive behavioural therapy of major depressive disorder. *Psychiatry Res*. 2014;223(2):164-170.
46. Ruf BM, Bhagwagar Z. The 5-HT1B receptor: a novel target for the pathophysiology of depression. *Curr Drug Targets*. 2009;10(11):1118-1138.
47. Bang-Andersen B, Ruhland T, Jørgensen M, et al. Discovery of 1-[2-(2,4-Dimethylphenylsulfanyl)phenyl]piperazine (Lu AA21004): A Novel Multimodal Compound for the Treatment of Major Depressive Disorder. *J Med Chem*. 2011;54(9):3206-3221.
48. Yang KC, Stepanov V, Amini N, et al. Effect of clinically relevant doses of vortioxetine and citalopram on serotonergic PET markers in the nonhuman primate brain. *Neuropsychopharmacology*. 2019;44:1706-1713.
49. Svenningsson P, Chergui K, Rachleff I, et al. Alterations in 5-HT1B receptor function by p11 in depression-like states. *Science*. 2006;311(5757):77-80.
50. Gerke V, Weber K. The regulatory chain in the p36-kd substrate complex of viral tyrosine-specific protein kinases is related in sequence to the S-100 protein of glial cells. *EMBO J*. 1985; 4(11):2917-20
51. Warner-Schmidt JL, Flajolet M, Maller A, et al. Role of p11 in Cellular and Behavioral Effects of 5-HT4 Receptor Stimulation. *J Neurosci*. 2009;29(6):1937-1946.
52. Lee KW, Westin L, Kim J, et al. Alteration by p11 of mGluR5 localization regulates depression-like behaviors. *Mol Psychiatry*. 2015;20(12):1546-1556.
53. Hessner F, Dlugos CP, Chehab T, et al. CC chemokine receptor 10 cell surface presentation in melanocytes is regulated by the novel interaction partner S100A10. *Sci Rep*. 2016;6:22649.
54. Rescher U, Gerke V. S100A10/p11: Family, friends and functions. *Pflugers Arch Eur J Physiol*. 2008;455:575-582.
55. Svenningsson P, Kim Y, Warner-Schmidt J, Oh YS, Greengard P. P11 and its role in depression and therapeutic responses to antidepressants. *Nat Rev Neurosci*. 2013;14:673-680.
56. Zokas L, Glenney JR. The calpactin light chain is tightly linked to the cytoskeletal form of calpactin I: Studies using monoclonal antibodies to calpactin subunits. *J Cell Biol*. 1987;105:2111-2121.
57. Milosevic A, Liebmann T, Knudsen M, Schintu N, Svenningsson P, Greengard P. Cell-

and region-specific expression of depression-related protein p11 (S100a10) in the brain. *J Comp Neurol*. 2017; 525(4):955-975

58. Su TP, Zhang L, Chung MY, et al. Levels of the potential biomarker p11 in peripheral blood cells distinguish patients with PTSD from those with other major psychiatric disorders. *J Psychiatr Res*. 2009;43:1078-1085.
59. Svenningsson P, Berg L, Matthews D, et al. Preliminary evidence that early reduction in p11 levels in natural killer cells and monocytes predicts the likelihood of antidepressant response to chronic citalopram. *Mol Psychiatry*. 2014;19(9):962-964.
60. Alexander B, Warner-Schmidt J, Eriksson T, et al. Reversal of depressed behaviors in mice by p11 gene therapy in the nucleus accumbens. *Sci Transl Med*. 2010;2(54). doi:10.1126/scitranslmed.3001079
61. Green H, Zhang X, Tiklova K, et al. Alterations of p11 in brain tissue and peripheral blood leukocytes in Parkinson's disease. *Proc Natl Acad Sci*. 2017;114(10):2735-2740.
62. Miller AH, Maletic V, Raison CL. Inflammation and Its Discontents: The Role of Cytokines in the Pathophysiology of Major Depression. *Biol Psychiatry*. 2009;65(9):732-741.
63. Syed SA, Beurel E, Loewenstein DA, et al. Defective Inflammatory Pathways in Never-Treated Depressed Patients Are Associated with Poor Treatment Response. *Neuron*. 2018;99:914-924.
64. Wittenberg GM, Greene J, Vértes PE, Drevets WC, Bullmore ET. Major Depressive Disorder Is Associated With Differential Expression of Innate Immune and Neutrophil-Related Gene Networks in Peripheral Blood: A Quantitative Review of Whole-Genome Transcriptional Data From Case-Control Studies. *Biol Psychiatry*. 2020;88(8):625-637.
65. Chen G, Emsor C, Russel D, Bohner B. The pharmacology of 1-(1-phenylcyclohexyl) piperidine-HCl. *J Pharmacol Exp Ther*. 1959;127(3):241-250.
66. Caddy C, Amit BH, McCloud TL, et al. Ketamine and other glutamate receptor modulators for depression in adults. *Cochrane database Syst Rev*. 2015;9:CD011612.
67. Lapidus KAB, Levitch CF, Perez AM, et al. A randomized controlled trial of intranasal ketamine in major depressive disorder. *Biol Psychiatry*. 2014; 76(12):970-6
68. Zarate CA, Singh JB, Carlson PJ, et al. A Randomized Trial of an NMDA antagonist in treatment-resistant major depression. *Arch Gen Psychiatry*. 2006;63:856-864.
69. Morgan CJA, Mofeez A, Brandner B, Bromley L, Curran HV. Acute Effects of Ketamine on Memory Systems and Psychotic Symptoms in Healthy Volunteers. *Neuropsychopharmacology*. 2004; 29(1):208-18
70. Yeung LY, Wai MSM, Fan M, et al. Hyperphosphorylated tau in the brains of mice and monkeys with long-term administration of ketamine. *Toxicol Lett*. 2010; 193(2):189-93
71. Maeng S, Zarate CA. The role of glutamate in mood disorders: Results from the ketamine in major depression study and the presumed cellular mechanism underlying its antidepressant effects. *Curr Psychiatry Rep*. 2007;9:467-474.
72. Zanos P, Gould TD. Mechanisms of ketamine action as an antidepressant. *Mol Psychiatry*. 2018;0:1-12.
73. Tyler MW, Yourish HB, Ionescu DF, Haggarty SJ. Classics in Chemical Neuroscience: Ketamine. *ACS Chem Neurosci*. 2017;8:1122-1134.
74. Du Jardin KG, Müller HK, Elfving B, Dale E, Wegener G, Sanchez C. Potential involvement of serotonergic signaling in ketamine's antidepressant actions: A critical review. *Prog Neuro-Psychopharmacology Biol Psychiatry*. 2016;71:27-38.

75. Du Jardin KG, Liebenberg N, Cajina M, et al. S-ketamine mediates its acute and sustained antidepressant-like activity through a 5-HT1B receptor dependent mechanism in a genetic rat model of depression. *Front Pharmacol*. 2018;8:978.
76. Yamanaka H, Yokoyama C, Mizuma H, et al. A possible mechanism of the nucleus accumbens and ventral pallidum 5-HT1B receptors underlying the antidepressant action of ketamine: a PET study with macaques. *Transl Psychiatry*. 2014;4(1):e342.
77. Sun HL, Zhou ZQ, Zhang GF, et al. Role of hippocampal p11 in the sustained antidepressant effect of ketamine in the chronic unpredictable mild stress model. *Transl Psychiatry*. 2016;6:e741.
78. Wharton J, Polak J. *Receptor Autoradiography: Principles and Practice*. Oxford University Press; 1993.
79. Attie AD, Raines RT. Analysis of receptor-ligand interactions. *J Chem Educ*. 1995;72(2):119-124.
80. Schmidt KC, Smith CB. Resolution, sensitivity and precision with autoradiography and small animal positron emission tomography: Implications for functional brain imaging in animal research. *Nucl Med Biol*. 2005;32(7):719-725.
81. Van Velden FH, Kloet RW, van Berckel BN, et al. HRRT versus HR+ human brain PET studies: an interscanner test-retest study. *J Nucl Med*. 2009;50(5):693-702.
82. Varrone A, Sjöholm N, Eriksson L, Gulyás B, Halldin C, Farde L. Advancement in PET quantification using 3D-OP-OSEM point spread function reconstruction with the HRRT. *Eur J Nucl Med Mol Imaging*. 2009;36:1639-1650.
83. Bé MM, Chisté V, Dulieu C, et al. *Table of Radionuclides, Comments on Evaluations 5. LNHB Report*. Vol. 1-5.; 2010.
84. Lee CM, Farde L. Using positron emission tomography to facilitate CNS drug development. *Trends Pharmacol Sci*. 2006;27(6):310-316.
85. Lundberg J, Tiger M, Landen M, Halldin C, Farde L. Serotonin transporter occupancy with TCAs and SSRIs: a PET study in patients with major depressive disorder. *Int J Neuropsychopharmacol*. 2012;15(8):1167-1172.
86. Farde L. The advantage of using positron emission tomography in drug research. *Trends Neurosci*. 1996;19:211-214.
87. Fletcher JW, Djulbegovic B, Soares HP, et al. Recommendations on the use of 18F-FDG PET in oncology. *J Nucl Med*. 2008;49(3):480-508.
88. Morris E, Chalkidou A, Hammers A, Peacock J, Summers J, Keevil S. Diagnostic accuracy of 18F amyloid PET tracers for the diagnosis of Alzheimer's disease: a systematic review and meta-analysis. *Eur J Nucl Med Mol Imaging*. 2016;43:375´4-385.
89. Pike VW. PET radiotracers: crossing the blood-brain barrier and surviving metabolism. *Trends Pharmacol Sci*. 2009;30(8):431-440.
90. Phelps ME, Hoffman EJ, Huang SC, Ter Pogossian MM. Effect of positron range on spatial resolution. *J Nucl Med*. 1975;16:649-652.
91. DeBenedetti S, Cowan CE, Konneker WR, Primakoff H. On the angular distribution of two-photon annihilation radiation. *Phys Rev*. 1950;77:205-212.
92. Gulyás B, Sjöholm N. Principles of Positron Emission Tomography. In: Hillary FG, De Luca J, eds. *Functional Neuroimaging in Clinical Populations*. The Guilford press; 2007:3-30.
93. Rousset OG, Ma Y, Evans AC. Correction for partial volume effects in PET: principle and validation. *J Nucl Med*. 1998;39(5):904-911.

94. Peng H, S. Levin C. Recent Developments in PET Instrumentation. *Curr Pharm Biotechnol*. 2010;11(6):555-571.
95. Boellaard R, Krak NC, Hoekstra OS, Lammertsma AA. Effects of noise, image resolution, and ROI definition on the accuracy of standard uptake values: A simulation study. *J Nucl Med*. 2004;45:1519-1527.
96. Innis RB, Cunningham VJ, Delforge J, et al. Consensus nomenclature for in vivo imaging of reversibly binding radioligands. *J Cereb Blood Flow Metab*. 2007;27:1533-1539.
97. Lammertsma AA. Compartmental Modeling in Emission Tomography. In: Grupen C, Buvat I, eds. *Handbook of Particle Detection and Imaging*. Springer Berlin Heidelberg; 2012:1065-1081.
98. Ichise M, Meyer JH, Yonekura Y. An introduction to PET and SPECT neuroreceptor quantification models. *J Nucl Med*. 2001;42:755-763.
99. Varnäs K, Varrone A, Farde L. Modeling of PET data in CNS drug discovery and development. *J Pharmacokinet Pharmacodyn*. 2013;40:267-279.
100. Lammertsma AA, Hume SP. Simplified reference tissue model for PET receptor studies. *Neuroimage*. 1996;4(3 Pt 1):153-158.
101. McCarthy T, Hoglund U, Antoni G, et al. Discovery and qualification of the first selective 5-HT1B PET radiotracer using a novel PET radiotracer development paradigm. In: *Paper Presented at the Joint Molecular Imaging Conference, Providence, Rhode Island, USA*. ; 2007.
102. Pierson ME, Andersson J, Nyberg S, et al. [11C]AZ10419369: A selective 5-HT1B receptor radioligand suitable for positron emission tomography (PET). Characterization in the primate brain. *Neuroimage*. 2008;41(3):1075-1085.
103. Saricicek A, Chen J, Planeta B, et al. Test-retest reliability of the novel 5-HT1B receptor PET radioligand [11C]P943. *Eur J Nucl Med Mol Imaging*. 2014;42(3):468-477.
104. Nord M, Finnema SJ, Schain M, Halldin C, Farde L. Test-retest reliability of [11C]AZ10419369 binding to 5-HT 1B receptors in human brain. *Eur J Nucl Med Mol Imaging*. 2014;41(2):301-307.
105. Lindberg A, Nag S, Schou M, et al. [11C]AZ10419096 – a full antagonist PET radioligand for imaging brain 5-HT1B receptors. *Nucl Med Biol*. 2017;54:34-40.
106. Gallezot JD, Nabulsi N, Neumeister A, et al. Kinetic modeling of the serotonin 5-HT(1B) receptor radioligand [(11)C]P943 in humans. *J Cereb Blood Flow Metab*. 2010;30(1):196-210.
107. Nord M, Finnema SJ, Halldin C, Farde L. Effect of a single dose of escitalopram on serotonin concentration in the non-human and human primate brain. *Int J Neuropsychopharmacol*. 2013;16(7):1577-1586.
108. Finnema SJ, Varrone A, Hwang T-J, Halldin C, Farde L. Confirmation of fenfluramine effect on 5-HT(1B) receptor binding of [(11)C]AZ10419369 using an equilibrium approach. *J Cereb Blood Flow Metab*. 2012;32(4):685-695.
109. Yang KC, Takano A, Halldin C, Farde L, Finnema SJ. Serotonin concentration enhancers at clinically relevant doses reduce [11C]AZ10419369 binding to the 5-HT1B receptors in the nonhuman primate brain. *Transl Psychiatry*. 2018;8(132).
110. Cosgrove KP, Kloczynski T, Nabulsi N, et al. Assessing the sensitivity of [11C]p943, a novel 5-HTIB radioligand, to endogenous serotonin release. *Synapse*. 2011;65(10):1113-1117.

111. Ridler K, Plisson C, Rabiner EA, et al. Characterization of in vivo pharmacological properties and sensitivity to endogenous serotonin of [11C] P943: A positron emission tomography study in Papio anubis. *Synapse*. 2011;65(11):1119-1127.
112. Varnäs K, Hall H, Bonaventure P, Sedvall G. Autoradiographic mapping of 5-HT1B and 5-HT1D receptors in the post mortem human brain using [3H]GR 125743. *Brain Res*. 2001;915(1):47-57.
113. Varnäs K, Halldin C, Hall H. Autoradiographic distribution of serotonin transporters and receptor subtypes in human brain. *Hum Brain Mapp*. 2004;22(3):246-260.
114. Fazio P, Schain M, Varnäs K, Halldin C, Farde L, Varrone A. Mapping the distribution of serotonin transporter in the human brainstem with high-resolution PET: Validation using postmortem autoradiography data. *Neuroimage*. 2016;133:313-320.
115. Schain M, Tóth M, Cselényi Z, et al. Improved mapping and quantification of serotonin transporter availability in the human brainstem with the HRRT. *Eur J Nucl Med Mol Imaging*. 2013;40(2):228-237.
116. Bonaventure P, Schotte A, Cras P, Leysen JE. Autoradiographic mapping of 5-HT1B- and 5-HT1D receptors in human brain using [3H]alniditan, a new radioligand. *Recept Channels*. 1997;5(3-4):225-230.
117. Torrey EF, Webster M, Knable M, Johnston N, Yolken RH. The Stanley Foundation brain collection and Neuropathology Consortium. *Schizophr Res*. 2000;44(2):151-155.
118. Maier DL, Sobotka-Briner C, Ding M, et al. [N-methyl-3H3]AZ10419369 binding to the 5-HT1B receptor: in vitro characterization and in vivo receptor occupancy. *J Pharmacol Exp Ther*. 2009;330(1):342-351.
119. Dubois A, Hérard A-S, Delatour B, et al. Detection by voxel-wise statistical analysis of significant changes in regional cerebral glucose uptake in an APP/PS1 transgenic mouse model of Alzheimer's disease. *Neuroimage*. 2010;51(2):586-598.
120. Schneider CA, Rasband WS, Eliceiri KW. NIH Image to ImageJ: 25 years of image analysis. *Nat Methods*. 2012;9(7):671-675.
121. Dubois A, Dauguet J, Delzescaux T. Ex Vivo and In Vitro Cross Calibration Methods. In: Kiessling F, Pichler BJ, eds. *Small Animal Imaging: Basics and Practical Guide*. Springer Berlin Heidelberg; 2011:317-346.
122. Evans AC, Collins DL, Millst SR, Brown ED, Kelly RL, Peters TM. 3D statistical neuroanatomical models from 305 MRI volumes. In: *IEEE-Nuclear S. Symposium, and Medical Imaging Conference*. ; 1993:1813-1817.
123. Tiger M, Svenningsson P, Nord M, Jabre S, Halldin C, Lundberg J. No correlation between serotonin and its metabolite 5-HIAA in the cerebrospinal fluid and [11C]AZ10419369 binding measured with PET in healthy volunteers. *Synapse*. 2014;68(10):480-483.
124. Varnäs K, Jučaite A, McCarthy DJ, et al. A PET study with [11C]AZ10419369 to determine brain 5-HT1B receptor occupancy of zolmitriptan in healthy male volunteers. *Cephalalgia*. 2013;33(10):853-860.
125. Varrone A, Svenningsson P, Forsberg A, et al. Positron emission tomography imaging of 5-hydroxytryptamine1B receptors in Parkinson's disease. *Neurobiol Aging*. 2014;35(4):867-875.
126. Sheehan D V., Lecrubier Y, Sheehan KH, et al. The Mini-International Neuropsychiatric Interview (M.I.N.I.): The development and validation of a structured diagnostic psychiatric interview for DSM-IV and ICD-10. *J Clin Psychiatry*. 1998;59(SUPPL.

20):22-33.
127. Schain M, Tóth M, Cselényi Z, et al. Quantification of serotonin transporter availability with [11C]MADAM — A comparison between the ECAT HRRT and HR systems. *Neuroimage*. 2012;60(1):800-807.
128. Nelder JA, Mead R. A Simplex Method for Function Minimization. *Comput J*. 1965;7(4):308-313
129. Cselényi Z, Olsson H, Halldin C, Gulyás B, Farde L. A comparison of recent parametric neuroreceptor mapping approaches based on measurements with the high affinity PET radioligands [11C]FLB 457 and [11C]WAY 100635. *Neuroimage*. 2006;32(4):1690-1708.
130. Jenkinson M, Beckmann CF, Behrens TEJ, Woolrich MW, Smith SM. FSL. *Neuroimage*. 2012;62(2): 782-790
131. Smith SM. Fast robust automated brain extraction. *Hum Brain Mapp*. 2002;17(3):143-155.
132. Jenkinson M, Bannister P, Brady M, Smith S. Improved Methods for the Registration and Motion Correction of Brain Images. *Neuroimage*. 2002;17:825-841.
133. Andersson JLR, Jenkinson M, Smith S. *Non-Linear Registration, Aka Spatial Normalisation. FMRIB Technial Report TR07JA2.*; 2007.
134. Castro ME, Pascual J, Romón T, del Arco C, del Olmo E, Pazos A. Differential Distribution of [3H]Sumatriptan Binding Sites (5-HT1B, 5-HT1D and 5-HT1F Receptors) in Human Brain: Focus on Brainstem and Spinal Cord. *Neuropharmacology*. 1997;36(4):535-542.
135. Baker KG, Halliday GM, Törk I. Cytoarchitecture of the human dorsal raphe nucleus. *J Comp Neurol*. 1990;301(2):147-161.
136. Schain M, Tóth M, Cselényi Z, et al. Improved mapping and quantification of serotonin transporter availability in the human brainstem with the HRRT. *Eur J Nucl Med Mol Imaging*. 2013;40(2):228-237.
137. Fazio P, Schain M, Varnäs K, Halldin C, Farde L, Varrone A. Mapping the distribution of serotonin transporter in the human brainstem with high-resolution PET: Validation using postmortem autoradiography data. *Neuroimage*. 2016;133:313-320.
138. Cecchetti L, Ricciardi E, Handjaras G, Kupers R, Ptito M, Pietrini P. Congenital blindness affects diencephalic but not mesencephalic structures in the human brain. *Brain Struct Funct*. 2016;221:1465-1480.
139. Chen Z, Chen X, Liu M, Liu S, Ma L, Yu S. Volume gain of periaqueductal gray in medication-overuse headache. *J Headache Pain*. 2017;18(12).
140. Kranz GS, Hahn A, Savli M, Lanzenberger R. Challenges in the differentiation of midbrain raphe nuclei in neuroimaging research. *Proc Natl Acad Sci U S A*. 2012;109(29):E2000-E2000.
141. Murty VP, Shermohammed M, Smith D V., Carter RMK, Huettel SA, Adcock RA. Resting state networks distinguish human ventral tegmental area from substantia nigra. *Neuroimage*. 2014;100:580-589.
142. Mizrahi O, Ish Shalom E, Baniyash M, Klieger Y. Quantitative Flow Cytometry: Concerns and Recommendations in Clinic and Research. *Cytom Part B - Clin Cytom*. 2018;94B:211-218.
143. Telford WG, Babin SA, Khorev S V., Rowe SH. Green fiber lasers: An alternative to traditional DPSS green lasers for flow cytometry. *Cytom Part A*. 2009;75(12):1031-9

144. Roederer M. Spectral compensation for flow cytometry: Visualization artifacts, limitations, and caveats. *Cytometry*. 2001;45(3):194-205
145. Weir JP. Quantifying test-retest reliability using the intraclass correlation coefficient and the SEM. *J Strength Cond Res*. 2005;19(1):231-240.
146. Nord M, Cselenyi Z, Forsberg A, et al. Distinct regional age effects on [11C]AZ10419369 binding to 5-HT1B receptors in the human brain. *Neuroimage*. 2014;103:303-308